Máster interuniversitario en mejora genética animal y biotecnología de la reproducción

Epigenetic changes and phenotypic impact through successive applications of a program of embryo vitrification

Alba Cano Vicent

Tutor: Francisco Marco Jiménez

2019/2020

Summary

The assisted reproductive technologies (ART) are increasingly used. However, in the last years, several studies have demonstrated the harmful effects associated with ART. There are more and more epigenetic studies corroborate that this differences between ART individuals and naturally conceived individuals produce marks in the genome. The adaptations of the embryo to the suboptimal conditions and stress on account of the vitrification during the development programming have consequences even at neonatal period or adulthood. The presented study aimed to evaluate the impact through successive applications of an embryo vitrification procedure on growth pattern and DNA methylation in liver tissue at adulthood. Initially, 2 experimental populations were developed: one from vitrified embryos transferred to the surrogate mothers (VT) and other from naturally conceived animals (NC). In both experimental groups, females were artificially inseminated (AI) with semen of unrelated males from the same strain. In the VT group, 3 days after AI, the embryos were recovered, vitrified and then transferred to surrogate mothers by laparoscopy. Meanwhile, NC offspring were generated letting the females give birth after AI. When the animals of first generation (F0) were in reproductive age, they were used to establish the second generation (F1) with the same procedure. The same procedure was utilized to generate third generation (F2) with F1 animals. At F0, F1 and F2, after delivery, offspring were weighed at birth, 4, 9, and 20 weeks. Growth curves were also estimated by nonlinear regression using the Gompertz equation, well suited for rabbits. At 56 weeks of age, animals of F0 and F1 were euthanized and 10 liver samples for each generation (5 VT and 5 NC) were taken. Over this samples, epigenetic study was performed. Our data showed that in F0 and F2 VT offspring exhibited differences significantly in the growth pattern, but, in F1, the offspring present a similar growth pattern. DNA methylation analysis reveals differences in methylation pattern between VT and NC animals in both generations. The comparative epigenomic analysis revealed 406 differentially methylated regions (DMRs) in F0, of which 61.1% were hypomethylated in VTF0 samples compared to the NCF0 ones; and 570 DMRs in F1, of which 56.0% were hypomethylated in VTF1 samples compared to the NCF1 ones. In conclusion, embryonic manipulation during the vitrification process is linked with embryo phenotypic

adaptation detected at adulthood. The phenotypic variation during the vitrification process may be associated with alterations in the genome methylation patterns in the liver tissue. Further research is needed to validate the significance of this finding.

Resumen

Las tecnologías de reproducción asistida (ART) se usan cada vez más. Sin embargo, en los últimos años, varios estudios han demostrado efectos perjudiciales asociados con las ART. Cada vez hay más estudios epigenéticos que corroboran que estas diferencias entre individuos ART e individuos naturalmente concebidos producen marcas en el genoma. Las adaptaciones del embrión a condiciones subóptimas y estrés debidas a la vitrificación durante el programa de desarrollo, tiene consecuencias en el periodo neonatal y adulto. El presente estudio está dirigido a evaluar el impacto a través de sucesivas aplicaciones del procedimiento de vitrificación del embrión en el patrón de crecimiento y la metilación del DNA del tejido del hígado en el adulto. Inicialmente, se desarrollaron dos poblaciones experimentales: una de embriones vitrificados transferidos a madres subrogadas (VT) y otra de animales naturalmente concebidos (NC). En los dos grupos experimentales, las hembras fueron inseminadas artificialmente (AI) con semen de machos no relacionados del mismo grupo. En el grupo VT, 3 días después de la AI, los embriones fueron recuperados, vitrificados y entonces transferidos a madres subrogadas por laparoscopia. Mientras tanto, la descendencia del NC fue generada, dejando que las hembras parieran después de la AI. Cuando los animales de la primera generación (F0) estaban en edad reproductiva, fueron usados para establecer la segunda generación (F1) con el mismo procedimiento. Del mismo modo se utilizaron los animales de la F1 para generar la tercera generación (F2). En F0, F1 y F2, la descendencia se pesó al nacimiento, a las 4, 9 y 20 semanas. Las curvas de crecimiento fueron estimadas por regresión no lineal, utilizando la ecuación de Gompertz, adecuada para conejos. A las 56 semanas, los animales de la F0 y la F1 fueron sacrificados y se obtuvieron 10 muestras de hígado de cada generación (5 VT y 5 NC). Sobre las muestras, se realizó el estudio epigenético. Nuestros datos muestras que, en la F0 y la F2, la descendencia del VT exhibe diferencias significativas en el patrón de crecimiento; pero, en la F1, la descendencia presenta un patrón de crecimiento similar. El análisis de metilación del DNA revela diferencias en el patrón de metilación entre los animales de VT y NC en ambas generaciones. El análisis epigenómico comparativo revela 406 regiones diferencialmente metiladas (DMRs) en F0, de

las cuales 61,1% son hipometiladas en las muestras VTF0 al compararlas con NCF0. Hay 570 DMRs en F1, de los cuales 56,0% son hipometiladas en las muestras de VTF1 al compararlas con las de NCF1. En conclusión, la manipulación embrionaria durante el proceso de vitrificación, está vinculada con adaptaciones del fenotipo del embrión, detectadas en el adulto. La variación del fenotipo durante el proceso de vitrificación podría estar asociado con alteraciones en el patrón de metilación del genoma en el tejido del hígado. Son necesarias futuras investigaciones para validar el significado de estos hallazgos.

Resum

Les tecnologies de reproducció assistida (ART) s'usen cada vegada més. No obstant això, en els últims anys, diversos estudis han demostrat efectes perjudicials associats amb les ART. Cada vegada hi ha més estudis epigenètics que corroboren que estes diferències entre individus ART i individus naturalment concebuts produïxen marques en el genoma. Les adaptacions de l'embrió a condicions subòptimes i estrés degudes a la vitrificació durant el programa de desenvolupament, tenen conseqüències en el període neonatal i adult. El present estudi està dirigit a avaluar l'impacte a través de successives aplicacions del procediment de vitrificació de l'embrió en el patró de creixement i la metilació del DNA del teixit del fetge en l'adult. Inicialment, es van desenrotllar dos poblacions experimentals: una d'embrions vitrificats transferits a mares subrogades (VT) i una altra d'animals naturalment concebuts (NC). En els dos grups experimentals, les femelles van ser inseminades artificialment (AI) amb semen de mascles no relacionats del mateix grup. En el grup VT, 3 dies després de l'AI, els embrions van ser recuperats, vitrificats i llavors transferits a mares subrogades per laparoscopia. Mentrestant, la descendència del NC va ser generada, deixant que les femelles pariren després de l'AI. Quan els animals de la primera generació (F0) estaven en edat reproductiva, van ser usats per a establir la segona generació (F1) amb el mateix procediment. De la mateixa manera es van utilitzar els animals de la F1 per a generar la tercera generació (F2). En F0, F1 i F2, la descendència es va pesar al naixement, a les 4, 9 i 20 setmanes. Les corbes de creixement van ser estimades per regressió no lineal, utilitzant l'equació de Gompertz, adequada per a conills. A les 56 setmanes, els animals de la F0 i la F1 van ser sacrificats i es van obtindre 10 mostres de fetge de cada generació (5 VT i 5 NC). Sobre les mostres, es va realitzar l'estudi epigenètic. Les nostres dades mostres que, en la F0 i la F2, la descendència del VT exhibix diferències significatives en el patró de creixement; però, en la F1, la descendència presenta un patró de creixement semblant. L'anàlisi de metilació del DNA revela diferències en el patró de metilació entre els animals de VT i NC en ambdós generacions. L'anàlisi epigenómic comparatiu revela 406 regions diferencialment metiladas (DMRs) en F0, de les quals 61,1% són hipometilades en les mostres VTF0 al comparar-les amb NCF0. Hi ha 570 DMRs en F1, dels

quals 56,0% són hipometilades en les mostres de VTF1 al comparar-les amb les de NCF1. En conclusió, la manipulació embrionària durant el procés de vitrificació, està vinculada amb adaptacions del fenotip de l'embrió, detectades en l'adult. La variació del fenotip durant el procés de vitrificació podria estar associat amb alteracions en el patró de metilació del genoma en el teixit del fetge. Són necessàries futures investigacions per a validar el significat d'estes troballes.

Index

1. Introduction

Since 1978, when the first human was conceived through in vitro fertilisation (Steptoe and Edwards, 1978), the assisted reproductive technologies (ART) are increasingly used (Charni-Natan et al., 2019). In 2018, it estimated that 1.6 million of the 5.4 million babies born in the world are conceived by ART (Adamson et al., 2018). Therefore, the total of embryos collected or produced in vitro goes up each age. For instance, in 2018, 1.499.367 cattle embryos were transferable, 0.8% more than 2017 (Viana, 2019). In breading, these technologies have a positive impact because shortening the generational interval, and it's a proper recourse to propagate the genetic around the world (Urrego et al., 2014). Additionally, animal models in ART are essential to reproductive and biomedical research (Stout, 2019). In the last years, several studies have demonstrated the harmful effects associated with ART (Feuer and Rinaudo, 2016; Duranthon and Chavatte-Palmer, 2018; Ramos-Ibeas et al., 2019). The offsprings born after the use of ARTs presented a low birth weight (Schieve et al., 2002), IGF concentration higher (Green et al., 2013), glucose intolerance (Calle et al., 2012), premature birth (Sirard, 2017), vascular dysfunction (Vroomar and Bartolomei, 2017) and congenital abnormalities (Waal et al., 2015), among others. Moreover, the application of ART in breading or in animal models confirm the difference between control and offspring born by ART (Ecker et al., 2004; Fernandez-Gonzalez et al., 2004:2010; Fauque et al., 2010; Feuer et al., 2017). For instance, less litter size (Donjacour et al., 2014), more fat mass at adulthood (Feuer and Rinaudo, 2017), high weight at adulthood (Gu et al., 2018) and metabolism and transporter lipid affected (Wang et al., 2013; Li et al., 2016).

The cryopreservation in ART mark a milestone due that high-quality embryos can be stored (Shaw et al., 2012). This technique has potential advantages such as preserving animal species (Goto et al., 2002), increasing live births rate (Wong et al., 2014) or keeping viable embryos for other transfer (Tachataki et al., 2003). Nevertheless, during the vitrification, the embryos are exposed to extreme conditions in the reprogramming period (Vrooman and Bartolomei, 2017, Ivanova et al., 2020). A growing body of evidence shows the effects in vitrified embryos due to the cryopreservation conditions (Vicente et al., 2013; Saenz-De-Juano et al., 2014:2015; Lavara et al., 2015). Some studies confirmed high fetal losses

and alterations in the development and placental formation of implanted cryopreserved embryos (Marco-Jimenez et al., 2013; Saenz-de-Juano et al., 2014). The adaptations of the embryo to the suboptimal conditions and stress on account of the vitrification during the development programming have consequences even at neonatal period or adulthood (Fleming et al., 2015; John and Rougeulle, 2018). The Developmental Origins of Health and Disease (DOHaD) hypothesis postulates that adaptions produce during critical periods in development, due to the plasticity, affect disease susceptibility (Roseboom, 2018; Lacagnina, 2019).

There are more and more epigenetic studies corroborate that this differences between ART individuals and naturally conceived individuals produce marks in the genome (Canovas et al., 2017; Hutanu et al., 2019; Kindsfather et al., 2019; La Rovere et al., 2019; Novakovic et al., 2019; Mani et al., 2020; Garcia-Dominguez et al., 2020). In 2002, Leese et al. Goldilocks' proposed principle, which could explain that early embryos show a remarkable flexible homeostatic mechanism to allow for the capacity to upregulate or downregulate metabolism in response to stress within the optimum (Leese et al., 2016). The extreme perturbation is surpassing the optimum, which shifts metabolism irreversibly. In vitro culture conditions produce epigenetic modification related to larger animals which suffer large offspring syndrome in sheep or cattle (Franzago et al., 2019). Futhermore, Chen et al., (2020) showed a disturbance in the epigenome of freeze-thawing individuals which affect the immune system and increase the risk of cancer later in life. Besides, the vitrification of germ cells o the manipulation of embryo exhibited different expression genes in comparative with natural reproduction (Wang et al., 2017; Ortiz-Rodriguez et al., 2019; Conine et al., 2020). In addition, ART affects DNA methylation in a tissue-specific manner (Hiendleder et al., 2006). Waal et al. (2015) had demonstrated ART individuals revealed very low DNA methylation at the H19/IgF1 in brain and liver what it entails cardiovascular and metabolic diseases.

The presented study aimed to evaluate the impact through successive applications of an embryo vitrification procedure on growth pattern and DNA methylation in liver tissue at adulthood.

2. Material and methods

All chemicals, unless otherwise stated, were reagent-grade and purchased from Sigma-Aldrich Química S.A. (Alcobendas, Madrid, Spain). All the experimental procedures used in this study were performed in accordance with Directive 2010/63/EU EEC for animal experiments and reviewed and approved by the Ethical Committee for Experimentation with Animals of the Universitat Politècnica de València, Spain (research code: 2018/VSC/PEA/0116).

2.1. Animals

The experiment was carried out with rabbits from genetic maternal line based on New Zealand White from the Universitat Politècnica de València.

2.2. Experimental design

Figure 1 illustrates the experimental design. Initially, 2 experimental populations were developed: one from vitrified embryos transferred to the surrogate mothers (VT) and other from naturally conceived animals (NC). In both experimental groups, females were artificially inseminated (AI) with semen of unrelated males from the same strain. In the VT group, 3 days after AI, the embryos were recovered, vitrified and then transferred to surrogate mothers by laparoscopy. Meanwhile, NC offspring were generated letting the females give birth after AI. After delivery, offspring were weighed at birth, 4, 9, and 20 weeks. When the animals of first generation (F0) were in reproductive age, they were used to establish the second generation (F1) with the same procedure. The same procedure was utilized to generate third generation (F2) with F1 animals. At 56 weeks of age, animals were euthanized liver samples were taken. From the liver, 10 individual biopsies for first and second generations were obtained (5 VT and 5 NC). Over the same samples, epigenetic study was performed.

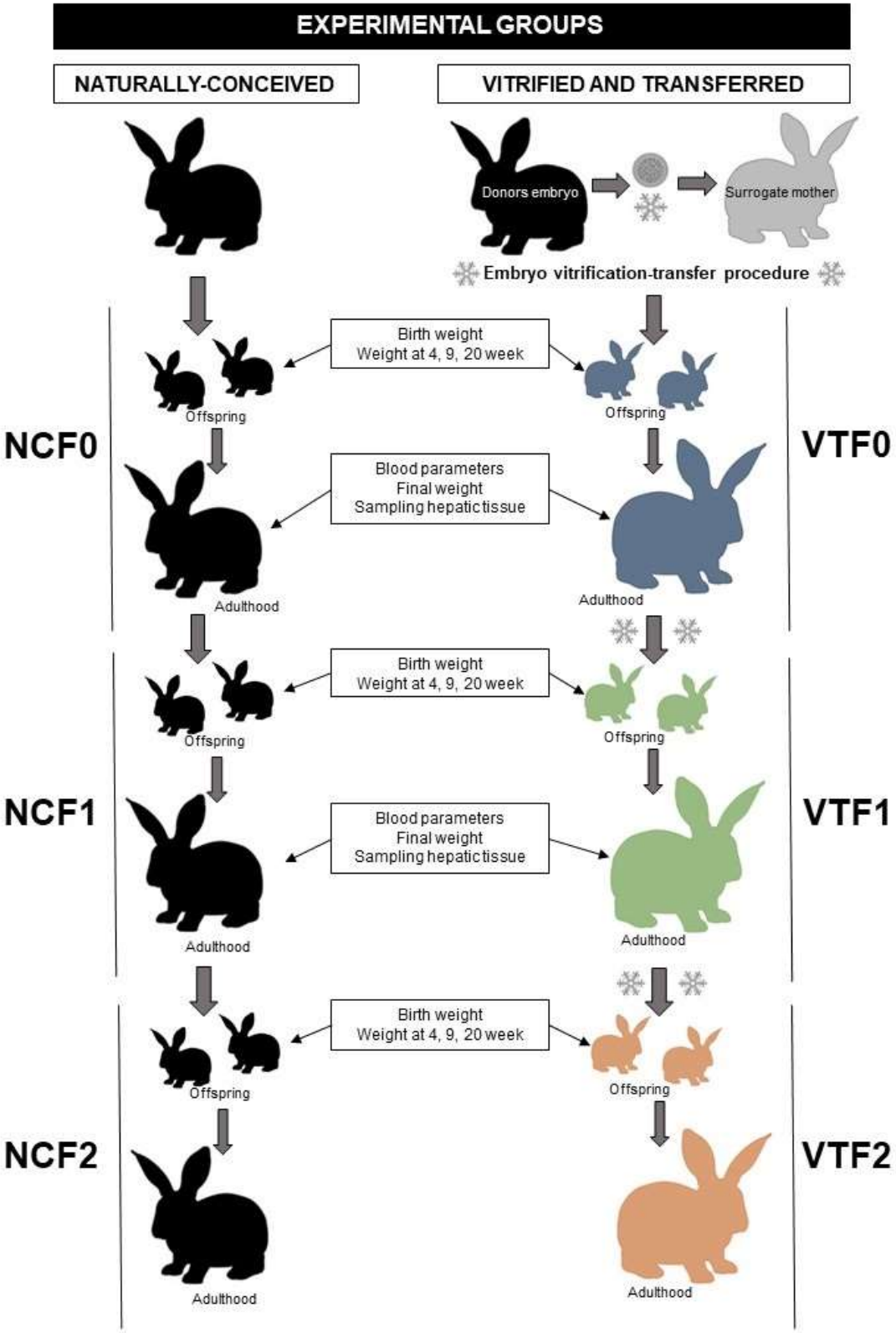

Figure 1. **Graphic representation of experimental design**

2.3. In vivo embryo production and collection

To establish F0, a total of 5 donors were AI with semen from fertile males. After that, ovulation was induced in the females by an intramuscular injection of 1 ug of burselin acetate. 72h post-AI, donors were euthanised. Embryos were recovered by perfusion of each oviduct and uterine horn with 5 mL pre-warmed (≈20-25ºC) Dulbecco's Phosphate-Buffered Saline (DPBS) supplemented with 0.2% of Bovine Serum Albumin (BSA), $CaCl_2$ (0.132 g/L) and antibiotics (penicillin 100 IU/mL, streptomycin 100 µg/mL and amphotericin B 0.25 µg/mL). After recovery (compacted morulae and early blastocysts), morphologically normal embryos (correct developmental stage, homogenous blastomeres and intact spherical mucin coat and zona pellucida) were selected and vitrified. A total of 101 embryos were vitrified to establish VTF0.

The procedure to obtained F1 and F2 was the same. To establish VTF1, 16 donors were AI with semen from 5 fertile males and a total of 310 embryos were vitrified. To establish VTF2, 19 donors were AI with semen from 8 fertile males and a total of 794 embryos were vitrified.

2.4. Vitrification and warming procedure

Embryos were vitrified and warmed using the methodology described by Vicente et al. (1999). The vitrification was carried out in two steps at room temperature (≈20-25 ºC). In the first step, embryos were placed for 2 min in a solution consisting of 10% (v/v) dimethyl sulphoxide (DMSO) and 10% (v/v) ethylene glycol (EG) in DPBS supplemented with 0.2% of BSA. In the second step, embryos were suspended for 30s in a solution of 20% DMSO and 20% EG in DPBS supplemented with 0.2% of BSA. Then, embryos suspended in vitrification medium were loaded into 0.125 mL plastic straws (French ministraw, IMV, L'Aigle, France) adding 2 sections of DPBS at either end of each straw, separated by air bubbles. Finally, straws were sealed and plunged directly into liquid nitrogen.

After storage in liquid nitrogen, warming was done by horizontally placing the straw 10 cm from liquid nitrogen for 20-30s and when the crystallisation process

began, the straws were immersed in a water bath at 20ºC for 10-15s. The vitrification medium was removed rinsing the embryos into a solution containing DPBS with 0.33 M sucrose for 5 min, followed by one bath in a solution of DPBS for another 5 min before transfer.

2.5. Embryo transfer by laparoscopy

Embryos were evaluated morphologically. Only embryos without damage in mucin coat or pellucid zone were transferred into the oviducts of 7 surrogate mothers by laparoscopy, following the procedure previously described by Besenfelder and Brem (1993). 68-72h before transfer, ovulation was induced in the surrogate mothers with an intramuscular dose of 1 µg Buserelin Acetate.

The mean number of transferred embryos per surrogate mothers was 14 in F0. During laparoscopy, surrogate mothers were anaesthetised by an intramuscular injection of xylazine (5 mg/Kg; Bayer AG) followed by an intravenous injection of ketamine hydrochloride (35 mg/Kg; Imalgene, Merial SA, Lyon, France) 5 min later. During laparoscopy, one dose of morphine hydrochloride (3 mg/Kg; Morfina, B. Braun, Barcelona, Spain) was administered intramuscularly. After surgery, animals were treated with antibiotics (4 mg/Kg of gentamycin each 24 h) and analgesics (0.03 mg/kg of buprenorphine hydrochloride each 12 h and 0.2 mg/kg of meloxicam every 24 h; Alvet Escarti S.L. Guadassuar, Spain) for 3 days. In the case of F1, 20 surrogate mothers were transfer with a mean of 16 embryos. In case of F2, 57 surrogate mothers were transfer with a mean of 16 embryos.

2.6. Control progeny

To generate NCF0, the AI was carried out using 0.5 mL of diluted fresh semen from fertile males. Immediately after that, ovulation was induced in the 6 inseminated females by an intramuscular injection of 1 ug of burselin acetate. When the animals of F0 were adults, the NCF1 were obtained with 15 NCF0 fertile males, which were used to inseminated 15 NCF0 females. To establish NCF2, 12 NCF1 fertile males were used to inseminated 14 NCF1 females.

2.7. Body growth and peripheral blood parameters study

In F0, a total of 216 animals (61 NCF0 and 155 VTF0) were weighed from birth to adulhood. In F1, a total of 251 animals (160 NCF1 and 91 VTF1) and in F2 a total of 1308 animals (867 NCF2 and 441 VTF2) were weighed in the same way that F0. Growth curves were also estimated by nonlinear regression using the Gompertz equation, well suited for rabbits (Blasco and Gomez, 1993): $y = a \exp[-b \exp(-kt)]$. Besides, individual blood samples were obtained in F0 and F1 animals and dispensed into a EDTA-coated tube (Deltalab S.L., Barcelona, Spain). Within 10 minutes of collection, samples were analysed using an automated veterinary haematology analyser MS 4e automated cell counter (MeletSchloesing Laboratories, France) according to the manufacturer's instructions. The blood parameters recorded were: white blood cells, lymphocytes, monocytes, granulocytes, red blood cells and haematocrit. Samples were processed in duplicate.

2.8. Sampling for the molecular signature of hepatic tissue

A total of 20 sample, 10 of F0 (5 VTF0 and 5 NCF0) and 10 of F1 (5 VTF1 and 5 NCF1), were generated obtaining some liver biopsies randomly. The samples were immediately washed with DPBS to remove blood remnants. Later that, each sample was stored in RNA-later (Ambion Inc., Huntingdon, UK) at -20 ºC. One day after, the sample are preserved at -80ºC for epigenome analysis.

2.9. Epigenome

The liver samples were processed by Molecular Biology Kit (BioBasic) to DNA extraction. About 15mg of liver were resuspended in 200ul of PBS and 200ul of CL to break the tissue with beads beater. Next, 50ul of proteinase K (20mg/ml) was added and incubated at 50ºC overnight. The next day, 20ul of RNase A was added and incubated 30min. After, 200ul EtOH 100% was added to the suspension and incubated at -20ºC for 2h. By last, the suspension was purified with CW1 and CW2 and was added 30ul CE buffer. DNA concentration and quality were estimated by Nanodrop and by agarose electrophoresis gel. After,

DNA samples were shipped to the Macrogen company (Seoul, South Korea). Methylated DNA was obtained using the MethylMiner Methylated DNA Enrichment kit (Invitrogen, Carlsbad, CA, USA) according to the manufacturer's instructions. Briefly, fragmentation of 1 µg of genomic DNA was performed using adaptive focused acoustic technology (AFA; Covaris) and captured by MBD proteins. The methylated DNA was eluted in high-salt elution buffer. DNA in each eluted fraction was precipitated using glycogen, sodium acetate, and ethanol, and resuspended in DNase-free water. The eluted DNA was used to generate libraries following the standard protocols of TruSeq Nano DNA Library Prep kit (Illumina). The eluted DNA was repaired, an A was ligated to the 3' end, and TruSeq adapters were ligated to the fragments. Once ligation was assessed, the adapter-ligated product was PCR amplified. The final purified product was quantified using qPCR according to the qPCR Quantification Protocol and qualified using Agilent Technologies 4200 TapeStation (Agilent technologies). We sequenced using the HiSeqTM 4000 platform (Illumina) and paired-end sequencing reads (101 bp) generated from MBD sequencing were verified using FastQC (version 0.10.0). Before starting the analysis, Trimmomatic (version 0.32) was used to remove any adapter sequences and bases with base qualities lower than 3 from the end reads. Using the sliding window trim method, bases that did not qualify for window size = 4 and mean quality = 15 were removed. Thereafter, reads with a minimum length of 36 bp were removed to produce clean data. Reads were mapped keeping strandness information against the reference genome for Oryctolagus cuniculus, version 2.0 from Ensembl using hisat2. Mapped data (SAM file format) were performed sorting and indexing using SAMtools (version 0.1.19).

Reads, whose bases were perfectly aligning against the genome and only align in unique region, were selected. The methylation ratio according to given Regions of Interest (ROI) is extracted from the alignment file using MEDIPS 1.38.0 R package (Lienhard, et al., 2013). The specified ROIs were promoter, gene, CDS, intron, 3' UTR and 5' UTR. Then, the resulting coverage profiles at each genomic bin were calculated as read count, Reads Per Kilobase Million (RPKM) and Relative Methylation Score (RMS). The sequences outcomes were processed by bioinformatics techniques to observed epigenetics differences between NC and

VT. Each differential methylated region (DMR), which were performed with exactTest function of edgeR, includes location of each gene, transcripts ID, gene ID, symbol gene and false change (FC). Only DMR with a threshold of a false change (FC) of > 1.5 and a p-valor < 0.05 were considered for further analyses.

ClustVis software was used to perform the Principal Component Analysis (PCA) of all expression data and the Heat-Map clustering (Metsalu and Vilo, 2015). Functional annotation of DMRs, enrichment analysis of their associated GO terms and KEGG pathways analysis were computed using the Bioinformatic software: David Functional Annotation Tool (version 6.8; October 2016), considering a P-value < 0.05.

2.10. Statistical analysis

A general linear model (GLM) was fitted for the Gompertz and blood parameters analysis, including as fixed effect the experimental group with 2 levels (VT and NC). The data are presented as least squares means ± standard error of means (NC-VT). Differences of $p<0.05$ were considered significant. Statistical analyses were performed with SPSS 21.0 software package.

3. Results

3.1. Body growth

In F0, the Gompertz growth curve describing a trend in which the growth decreased as vitrified embryonic manipulation. As estimated by the Gompertz equation (a parameter), this trend was also patent in late adulthood (5682,9 ± 127,72g, and 4014,7 ± 79,53g, for NCF0 and VTF0 groups, respectively; Figure 2).

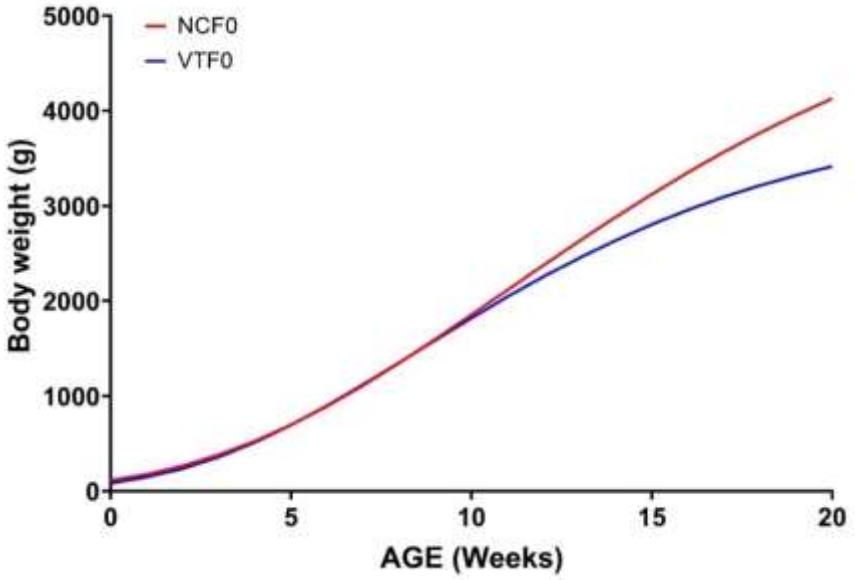

Figure 2. Growth curves of F0 generation: comparing differences between animals naturally conceived (NCF0) and those born after vitrified embryo transfer (VTF0) of first generation.

In F1, the Gompertz growth curve describing the same trend in the two groups. There wasn't significantly differences in late adulthood, as estimated by the Gompertz equation (a parameter) (Figure 3).

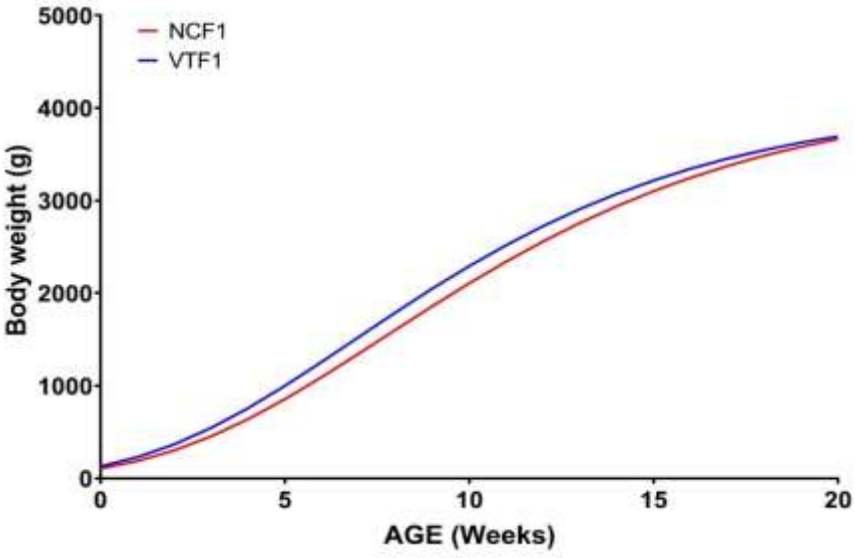

Figure 3. Growth curves of F1: comparing differences between animals naturally conceived (NCF1) and those born after vitrified embryo transfer (VTF1) of second generation.

In F2, the Gompertz growth curve describing the opposite trend of the F0, the growth increased as vitrified embryonic manipulation. As estimated by the Gompertz equation (a parameter), there was significantly differences in late adulthood between animals with embryonic manipulation and natural conceived animals (4047,6 ± 50,08g and 4549,4 ± 77,00, for NCF2 and VTF2 groups, respectively; Figure 4).

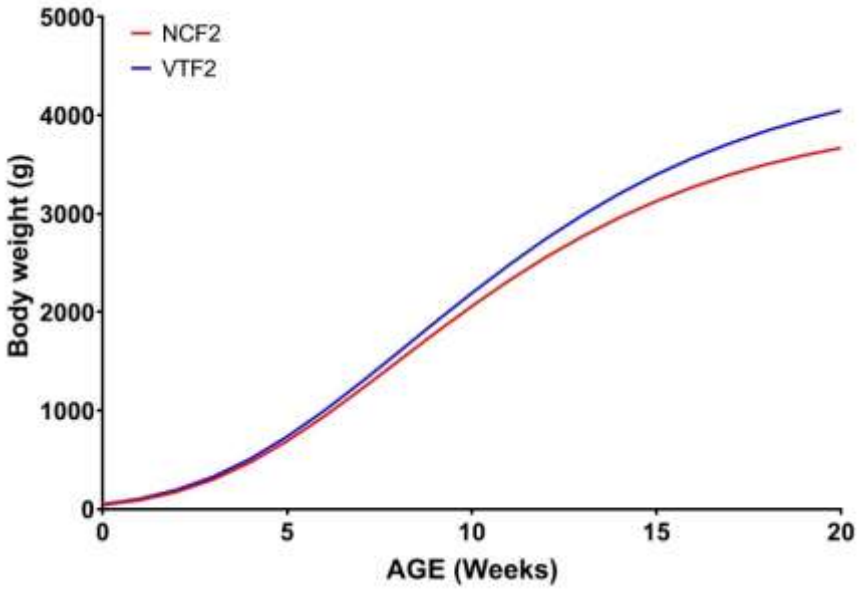

Figure 4. Growth curves of F2 generation: comparing differences between animals naturally conceived (NCF2) and those born after vitrified embryo transfer (VTF2) of third generation.

3.2. Vitrified embryo transfer procedure seems to be neutral on the peripheral blood parameters

As shown in Figure 5, there were no significant differences in peripheral profile of blood cells (white blood cells, red blood cells, and haematocrit), between VT and NC groups in F0 and F1.

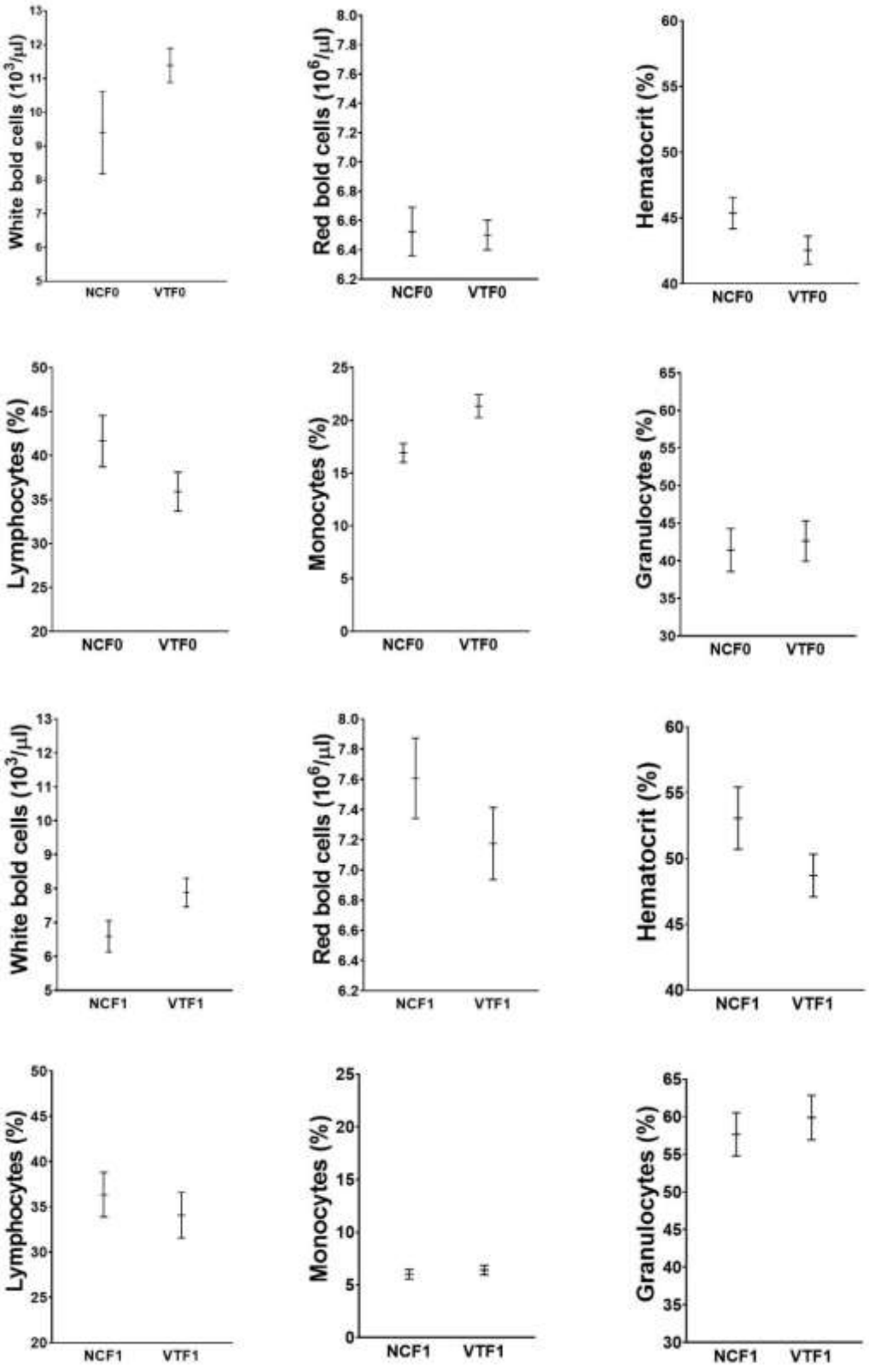

Figure 5. F0 and F1 peripheral profile of blood. Haematological comparison between VT and NC groups.

3.3. Genome-wide methylation changes in the liver of VT rabbits

MBD sequencing was performed on the NC and VT samples of the two generations. After quality verification and trimming procedure, about 19.3 million raw sequencing reads were generated from each sample. Reads, whose bases were perfectly aligning against the genome and only align in unique region, were selected (Table 1).

Table 1. Data generated by MBD-seq. Genome coverage as the percentage of bases mapped by genome-wide reads.

Group	Total number of raw sequence reads	Mapped reads in total reads (%)	Unique mapped reads (%)
NCF0	18695662,6 ± 36108,82	75,4 ± 3,41	65,4 ± 3,35
VTF0	19595867,7 ± 2254876,25	75,8 ± 2,68	64,8 ± 3,49
NCF1	19548044,4 ± 60920,63	75,6 ± 4,19	65,1 ± 4,84
VTF1	19438277,8 ± 57737,85	73,1 ± 2,23	62,4 ± 2,36

The methylation peaks identified in the specified ROIs (promoter, gene, CDS, intron, 3’ UTR and 5’ UTR) in F0 showed the highest density of methylated regions (MR) in 3’ UTR and the lower density of MR in Promoter (Figure 6a). PCA (Figure 6b) graphics revealed high methylation differences between VTF0 and NCF0 samples.

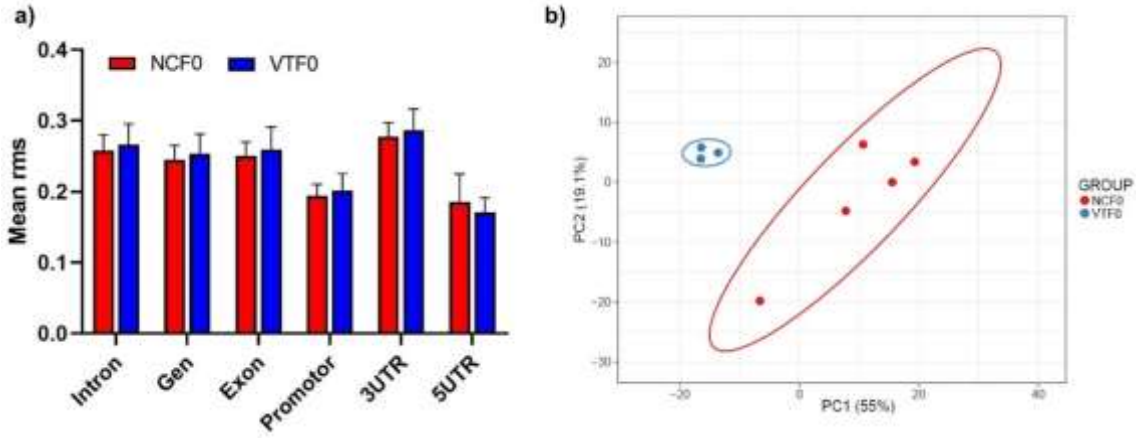

Figure 6. Genome-wide methylation changes in the liver of F0 animals after embryo cryopreservationtransfer procedure. Samples between vitrified-transferred (VTF0) and naturally-conceived (NCF0) group were compared. [a] Mean of rms in different genomic regions. [b] Principal Component Analysis of F0 which performed taking into account only DMRs.

The F0 MA-plot, scatter plot in a logarithmic scale of fold changes (y-axis) versus the mean expression signal (x-axis), confirm the high methylation differences between VTF0 and NCF0 samples (Figure 7a). The Heatmap graphic (Figure 7b), grouped the samples according to their origin.

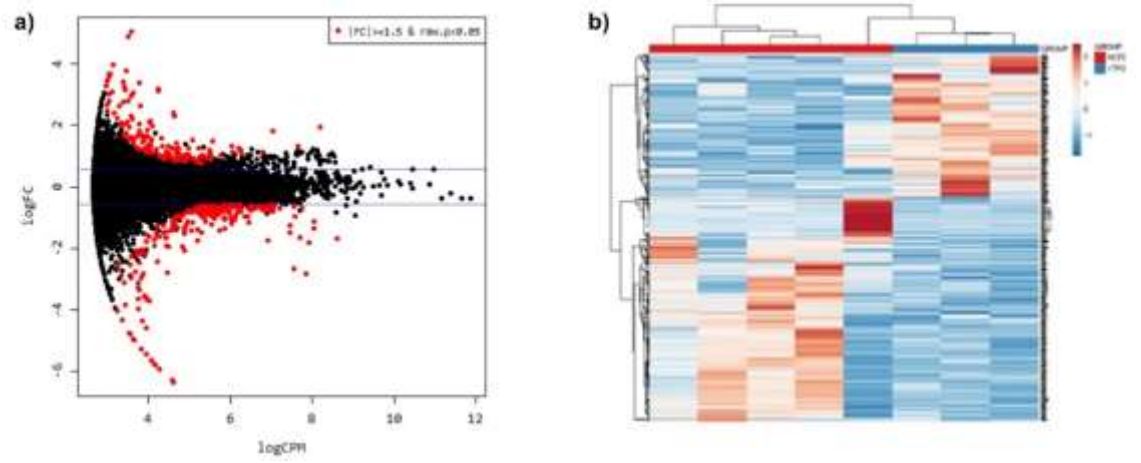

Figure 7. Genome-wide methylation changes in the liver of F0 animals after embryo cryopreservationtransfer procedure. Samples between vitrified-transferred (VTF0) and naturally-conceived (NCF0) group were compared. [a] MA plot representing data comparison between VTF0 and NCF0 samples. [b] Heat-Map clustering which performed taking into account only DMRs.

Of the 21 chromosomes in the rabbit genome and mitochondrial chromosome, 11 chromosomes had a significantly ($p<0.05$) different mean of counts between NCF0 and VTF0. In this way, 12 chromosomes were hypermethylated and 10 chromosomes were hypomethylated in the VTF0 group compared with NCF0. (Figure 8a). The comparative epigenomic analysis revealed 406 differentially methylated regions (DMRs), of which 61.1% were hypomethylated (248/406) and 38.9% hypermethylated (158/406) in VTF0 samples compared to the NCF0 ones (Figure 8b).

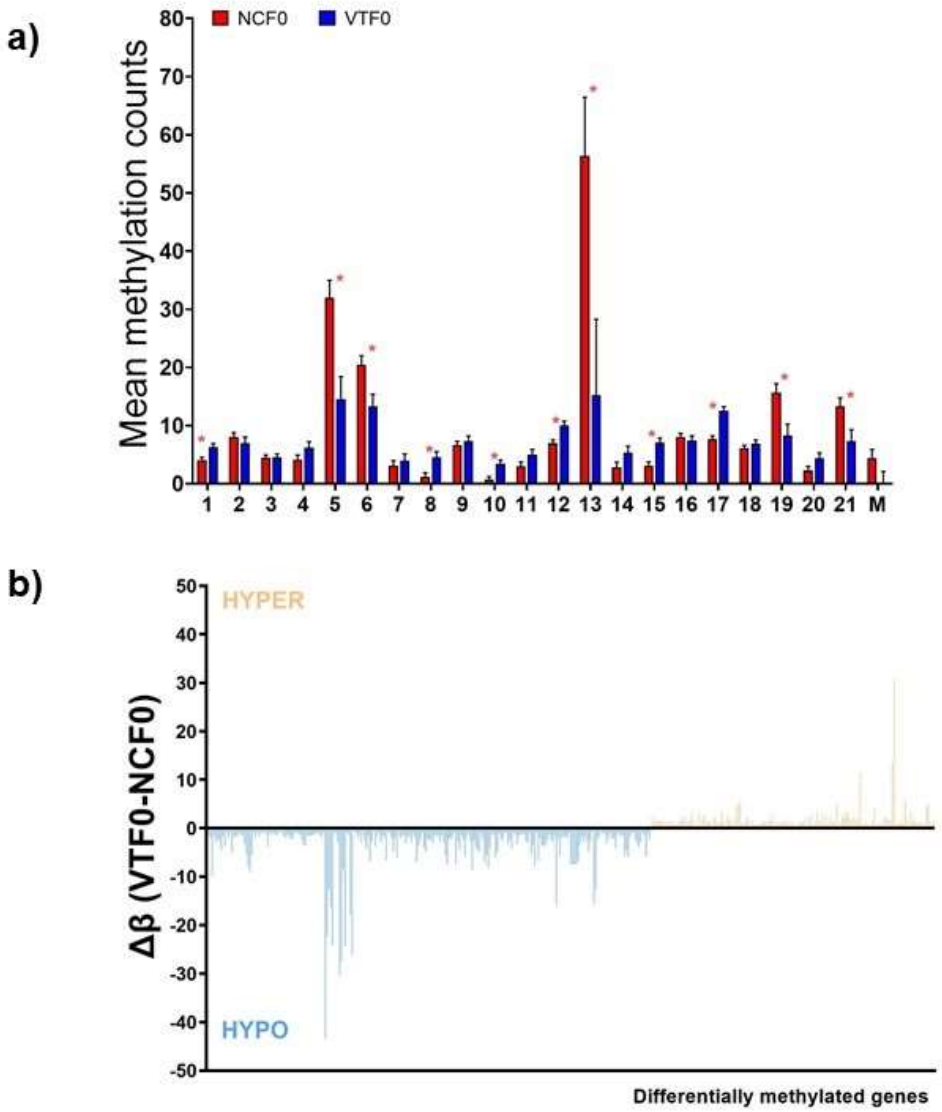

Figure 8. Genome-wide methylation changes in the liver of F0 animals after embryo cryopreservation transfer procedure. [A] Mean of methylation counts per chromosome. Asterisks denote statistical differences. [B] Methylation difference (Δβ) of the 406 DMRs calculated as mean VTF0 DNA methylation minus mean NCF0 DNA methylation.

From these DMRs, DAVID software recognises 368 genes, whose gene name and methylation difference (Δβ) were annotated in Annexed (Supplementary Table 1).

Functional analysis showed more GO due to hypomethylated DMRs than GO due to hypermethylated DMRs (Figure 9). The hypermethylated DMRs had relevant associations with ribosome and his composition in categories “Cellular component” and “Kegg” (Figure 9a, b). DAVID GO term enrichment and KEGG pathway analysis of both hypomethylated and hypermethylated genes are showed in Annexed (Supplementary Table 2).

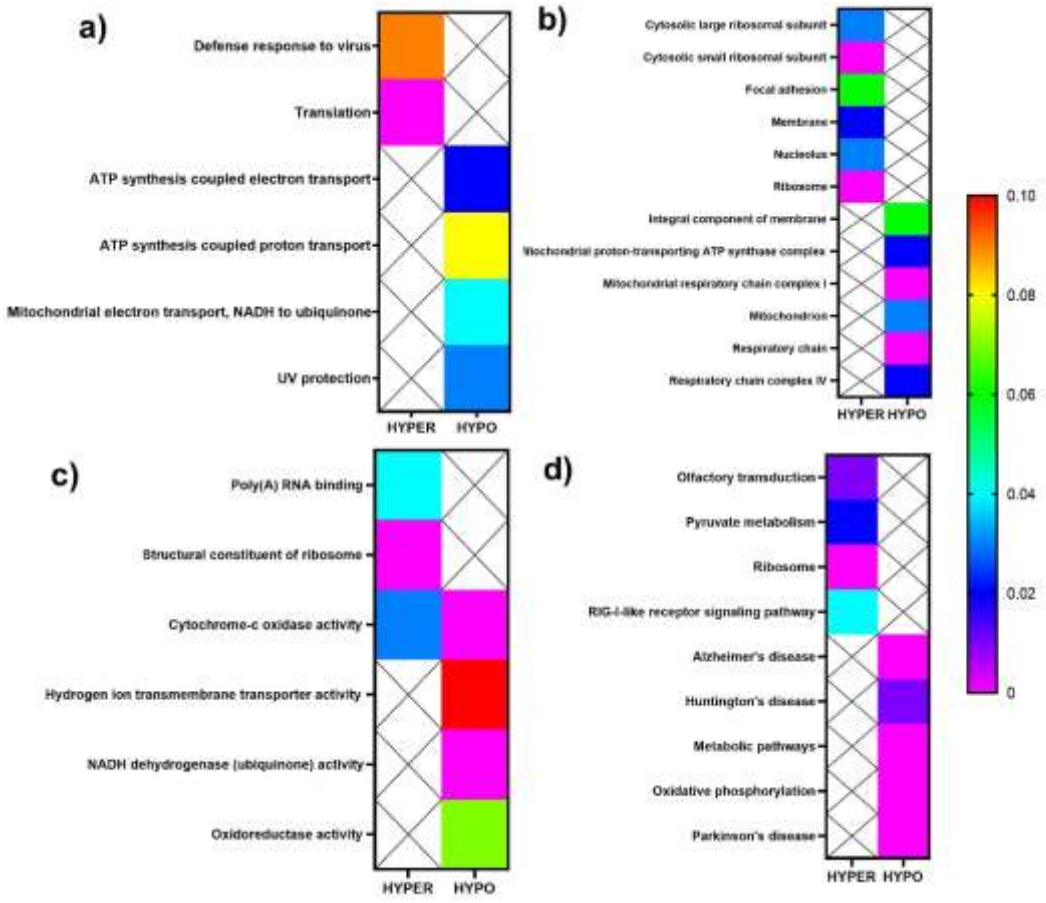

Figure 9. Gene ontology and KEGG analysis for the hyper- and hypo- DMRs of F0. [a] Biological Process [b] Cellular Component [c] Molecular Function [d] Kegg.

The methylation peaks identified in the specified ROIs (promoter, gene, CDS, intron, 3' UTR and 5' UTR) in F1 showed the highest density of methylated regions (MR) in 3' UTR and the lower density of MR in 5' UTR (Figure 10a). PCA (Figure 10b) graphics revealed high methylation differences between VTF1 and NCF1 samples.

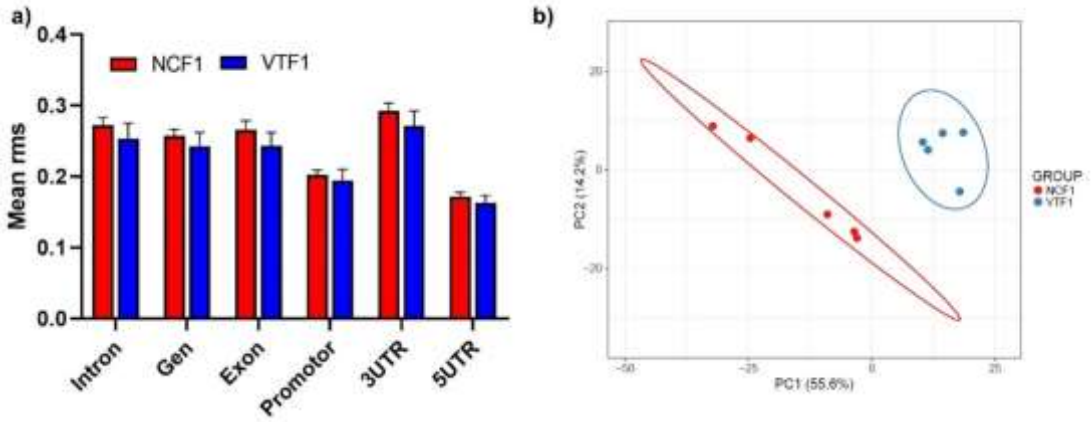

Figure 10. Genome-wide methylation changes in the liver of F1 animals after embryo cryopreservationtransfer procedure. Samples between vitrified-transferred (VTF1) and naturally-conceived (NCF1) group were compared. [a] Mean of rms in different genomic regions. [b] Principal Component Analysis of F1 which performed taking into account only DMRs.

The F1 MA-plot, scatter plot in a logarithmic scale of fold changes (y-axis) versus the mean expression signal (x-axis), confirm the high methylation differences between VTF1 and NCF1 samples (Figure 11a). The Heatmap graphic (Figure 11b), grouped the samples according to their origin.

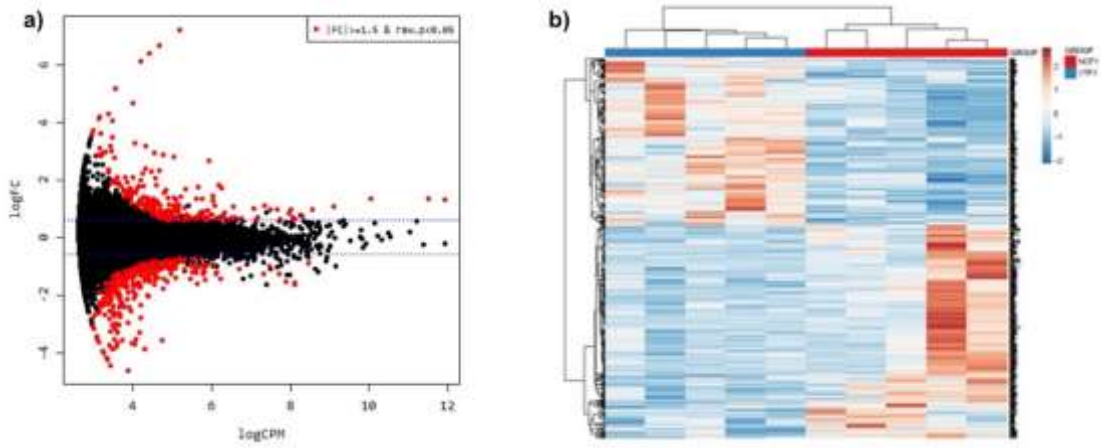

Figure 11. Genome-wide methylation changes in the liver of F1 animals after embryo cryopreservationtransfer procedure. Samples between vitrified-transferred (VTF1 and naturally-conceived (NCF1) group were compared. [a] MA plot representing data comparison between VTF1 and NCF1 samples. [b] Heat-Map clustering which performed taking into account only DMRs.

Of the 21 chromosomes in the rabbit genome and mitochondrial chromosome, 5 chromosomes had a significantly ($p<0.05$) different mean of counts between NCF1 and VTF1. In this way, 3 chromosomes were hypermethylated and 19 chromosomes were hypomethylated in the VTF1 group compared with NCF1 (Figure 12a). The comparative epigenomic analysis revealed 570 differentially methylated regions (DMRs), of which 56.0% were hypomethylated (319/570) and 44.0% hypermethylated (251/570) in VTF1 samples compared to the NCF1 ones (Figure 12b).

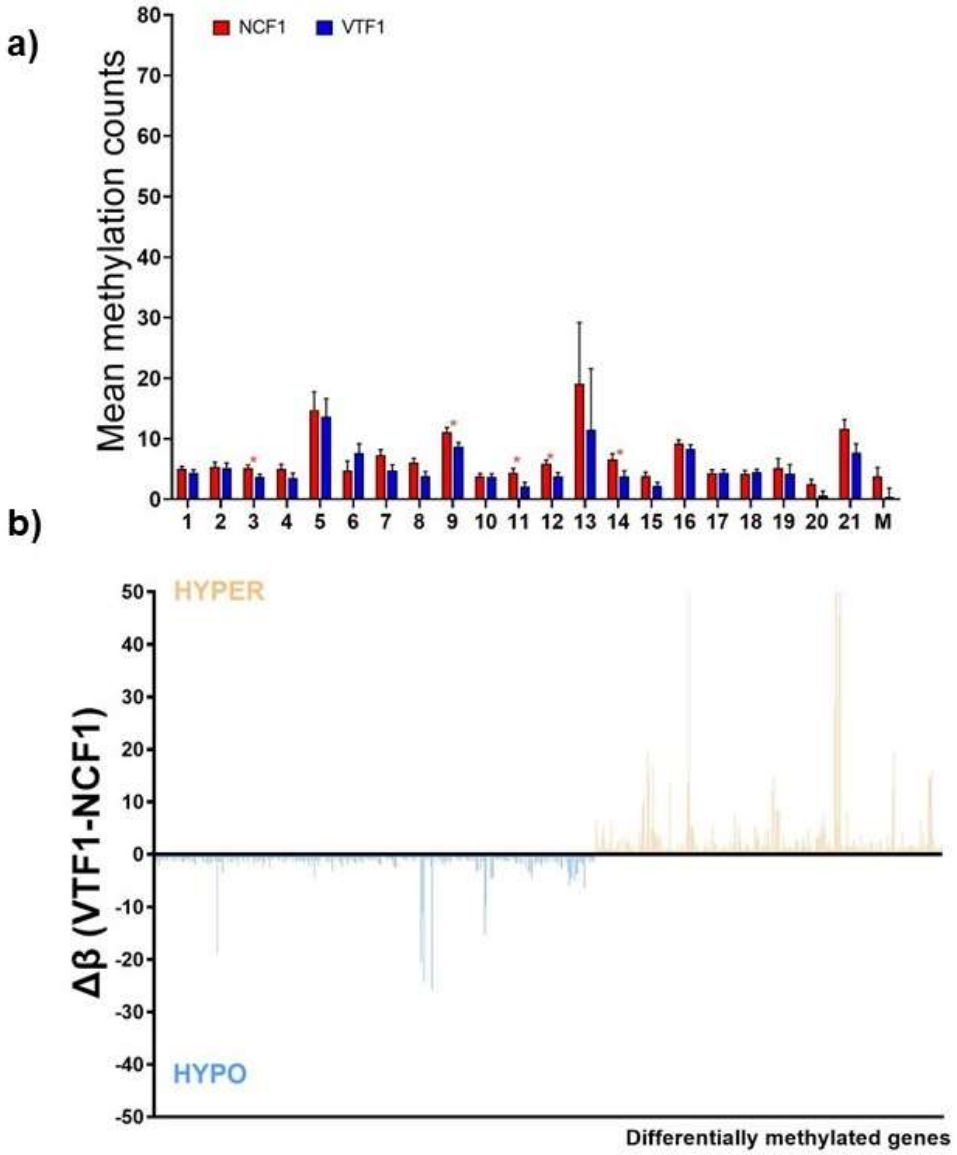

Figure 12. Genome-wide methylation changes in the liver of F1 animals after embryo cryopreservationtransfer procedure. Samples between vitrified-transferred (VTF1) and naturally-conceived (NCF1) group were compared. [A] Mean of methylation counts per chromosome. Asterisks denote statistical differences. [B] Methylation difference (Δβ) of the 570 DMRs calculated as mean VTF1 DNA methylation minus mean NCF1 DNA methylation.

From these DMRs, DAVID software recognises 484 genes, whose gene name, associated chromosome/scaffold and methylation difference (Δβ) were annotated in Annexed (Supplementary Table 3).

Functional analysis showed more GO due to hypomethylated DMRs than GO due to hypermethylated DMRs (Figure 13). The hypomethylated DMRs had relevant associations with ribosome and his composition in categories “Cellular component” and “Kegg” (Figure 13a, b). DAVID GO term enrichment and KEGG pathway analysis of both hypomethylated and hypermethylated genes are showed in Annexed (Supplementary Table 4).

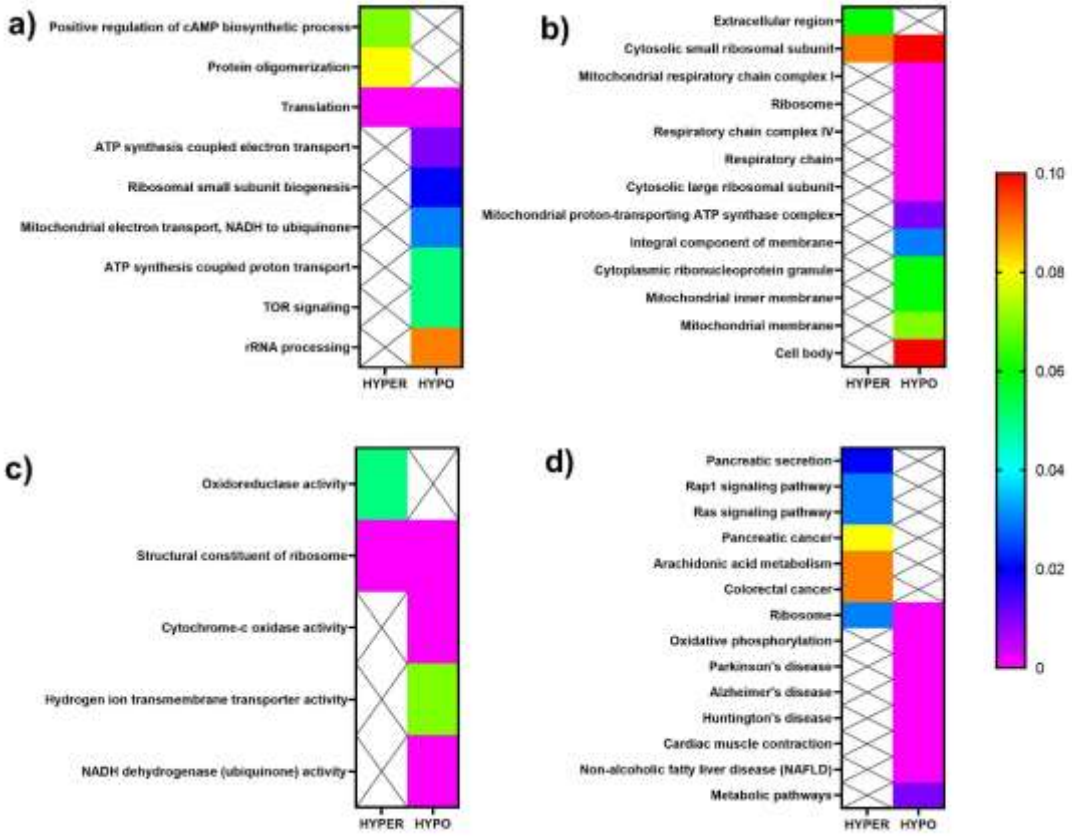

Figure 13. Gene ontology and KEGG analysis for the hyper- and hypo- DMGs of F1. [a] Biological Process [b] Cellular Component [c] Molecular Function [d] Kegg

4. Discussion

The present study reports, for the first time, that embryo responses to stress induced by vitrification procedure provide adaptative phenotypic changes that could be associated with the liver epigenetic pattern modification. We show that, compared to natural conceived, progeny born after embryo exposure to the vitrification procedure exhibited a difference in growth pattern from birth age to adulthood with no sign that it impacts on health. Nevertheless, the consequence of repeat stress across generations presents a changing trend of the growth pattern. We found a reverse pattern across generation, being the animals born after vitrification procedure lightweight compared to NC in the F0 generation to heavier in the F2 generation.

Mounting evidence suggests that ART manipulations are associated with phenotypic outcomes in human (Guo et al., 2017;; Chen et al., 2018; Duranthon and Chavatte-Palmer, 2018; Zandstra et al., 2018; Zhang et al., 2019) and other animals species (Ecker et al., 2004; Fernandez-Gonzalez et al., 2004:2010; Fauque et al., 2010; Feuer and Rinaudo, 2016; Feuer et al., 2017; Vrooman and Bartolomei, 2017; Ramos-Ibeas et al., 2019). Therefore, our study adds further evidence for the direct long-term effect of ART on phenotype. Bodyweight is used as phenotypic criteria for growth, and it is considered to reflect proliferative events during organogenesis and development (Winick and Noble, 1965). Till now, little data exist about the long-term effect of embryo cryopreservation on phenotype. We previously developed a cohort of studies, in a rabbit model under strictly regulated experimental conditions, linked embryo cryopreservation with short and long-term outcomes. We assessed gene expression in preimplantation embryos (Vicente et al., 2013; Saenz-De-Juano et al., 2014:2015; Lavara et al., 2015), the foetal and placental weights (Saenz-De-Juano et al., 2015), the offspring's growth pattern and adult body weight (Garcia-Dominguez et al., 2020; Lavara et al., 2015), the reproductive traits from derived females (Lavara et al., 2014). The present study provides new evidence confirming that embryo vitrification procedure incurs phenotypic changes throughout life, consistent with our previous results (Garcia-Dominguez et al., 2020). Specifically, animals born after vitrification procedure show a higher birth weight and poor growth performance.

In agreement, other studies show evidence that cryopreservation procedure incurs phenotypic changes throughout life, like differences in birth weight (Schieve et al., 2002; Chen et al., 2020) or the high body weight at adulthood (Gu et al., 2018).

Deviations in the growth pattern and phenotype have been described by several authors after ART, evidencing that different procedures applied to different genotypes would lead to different outcomes, probably through specific epigenetic modifications (Dulioust et al., 1995; Fernández-Gonzalez et al., 2004; Feuer et al., 2014a:b; Velazquez et al., 2018; Nusbaumer et al., 2019; Garcia-Dominguez et al., 2020). In the last years, epigenetic alterations have been invoked as a mechanistic candidate that might explain the association between ART and its associated outcomes throughout life (Marchesi et al., 2012; Kohda, 2013; Novakovic et al., 2019; Ivanova et al., 2020; Kohda and Ishino, 2013). Still, at present, the link between epigenetic modifications and long-term effects in terms of phenotype in ART offspring remains unclear. Previous studies have suggested that these epigenetic modifications are due to the adaptations of the embryo to extreme conditions, for example, the vitrification technique (Vrooman and Bartolomei, 2017). The epigenetic states are especially dynamics during the reprogramming period (Ivanova et al., 2020), coinciding with the vitrification time (Chen et al., 2020). The adaptations of the embryo to the suboptimal conditions and stress have consequences even at neonatal period or adulthood (Fleming et al., 2015; John and Rougeulle, 2018). Thus, stress during a critical period can modify the pattern of epigenetic marks can change (Canovas et al., 2017; Hutanu et al., 2019; Kindsfather et al., 2019; La Rovere et al., 2019; Mani et al., 2020). In this work, we found evidence of a difference in 'global' DNA methylation in liver tissue of VT and NC groups at adulthood. Thus, epigenetic analysis of F0 animals showed a total of 406 DMRs, with hypomethylated domains prevalent over hypermethylated domains in VTF0 samples compared to the NCF0 ones. Little data exist about the effects of ART on epigenetic variation; however, Novakovic et al. (2019) show evidence for specific ART-associated change in methylation around birth in humans. Using this approach, we found that 8.6% of DMRs were related to ribosomal protein genes (RPGs). Moreover, 29 of 35 affected RPGs

were hypermethylated, while 6 were hypomethylated. A similar direct effect of growth under stress with significant effects on the global amount of RPGs have been reported in *Saccharomyces cerevisiae* (Ghulam et al.,2020). Furthermore, in fish has been demonstrated that stress conditions (changes in temperature) produce high translation rates of ribosomal components, which may contribute to decreased animal growth (Windisch et al., 2014). Besides, based on transcriptomic analysis, has been described that fertilization with cryopreserved sperm downregulates ribosomal genes in embryo result in an embryonic retardation growth (Ortiz-Rodriguez et al., 2019), and in vitrified oocyte also downregulated ribosomal protein-related genes (Wang et al., 2017). Recently, Conine et al. (2020) provide ribosomal protein genes and other genes involved in ribosome biogenesis of differing ex vivo fertilization methods. Although the mechanism that explained differential susceptibility to cryopreservation in embryos is not understood (Marco-Jiménez et al., 2018), our findings suggest the activation of molecular mechanisms and cellular events involved in an adaptive response to the lethal effects of vitrification, with consequences in growth pattern.

Due to the widespread use of ART, some theories have emerged due to repercussion on offspring health and physiology. The Developmental Origins of Health and Disease (DOHaD) theory proposed a link between periconceptional, foetal and early infant phases of life and the long-term development of health disorders, which might be transgenerational (Roseboom, 2018; Lacagnina, 2019). Accordingly, the exposure of early embryos to environmental stressors has been linked to diabetes, obesity, heart disease, stroke, and other latent cardiometabolic diseases (Feuer and Rinaudo, 2016; Novakovic et al., 2019). Based on our results, we would rule out apparent health problems, at least in rabbits, in line with previous findings (Lavara et al., 2015; Marco-Jiménez et al., 2018). It was estimated that ART has contributed to the birth of over 8 million liveborn babies worldwide (Charni-Natan et al., 2019). Based on this dataset, we understand that alterations in the health do not appear to represent a problem for ART conceived due that any significant health problems should have already been described (Halliday et al., 2019). In 2002, Leese et al. Goldilocks' proposed principle, which could explain what seems to be happening with embryo

manipulation during the vitrification procedure. Early embryos show a remarkable flexible homeostatic mechanism to allow for the capacity to upregulate or downregulate metabolism in response to stress within the optimum (Leese et al., 2016). Thus, embryo homeostatic mechanism up or down within the optimum from which the embryo can overcome, while extreme perturbation surpassing the optimum which shifts metabolism irreversibly. Therefore, we utilized a novel multigenerational exposure paradigm to identify the effects of vitrification procedure during a vulnerable developmental window on phenotype across generations (F0, F1 and F2). We found evidence for an association between the vitrification procedure and growth pattern. While in F0 and F2 VT offspring exhibited differences significantly in the growth pattern, F1 offspring present a similar growth pattern. In combination, these data suggest a complex interplay in regulation the growth. Specifically, DNA methylation analysis identified differences in DNA methylation patterns were observed between VTF1 and NCF1 animals. Specifically, a different bimodal methylation landscape was present between VTF1 and NCF1, with hypomethylated domains prevalent over hypermethylated domains, similar to F0 generation. Nevertheless, while in F0 generation, there were 12 chromosomes hypermethylated and 10 hypomethylated, in F1 generation there were 19 chromosomes hypermethylated and 3 hypomethylated. Moreover, significant differences in the counts between NC and VT were observed in 11 chromosomes in the F0 generation, while this difference was found only in 5 chromosomes in the F1 generation. It should be noted that solely chromosome 12 was common amongst the two-generation. In terms of the DMRs, above 14.7% (71/484) were RPGs in F1. These data indicated a relevant increase of RPGs from F0 to F1, suggesting that they could partly explain the detected pattern variation in growth. Moreover, different patterns were manifest amongst RPGs, being more hypomethylated RPGs in F1 animals, while in F0 where more hypermethylated. As regards the functional analysis, the most GO implicated in RPGs (Ribosome, Cytosolic large ribosomal subunit, Cytosolic small ribosomal subunit) were common between hypermethylated genes in F0 and hypomethylated genes in F1 and vice versa. Despite further research being required, our data suggest that the vitrification procedure may act as selection tool ("cryoselection"), in which vitrification technique remove embryos that not survive stresses associated with the embryo

manipulation, allowing only the "resistant" ones generate offspring (Vidal 2017; Sallem et al., 2018; Marsico et al., 2019). Although the mechanism that explained differential susceptibility to cryopreservation in embryos is not understood, our findings suggest the activation of molecular mechanisms and cellular events involved in an adaptive response to the lethal effects of vitrification (Marco-Jiménez et al., 2018).

In conclusion, embryonic manipulation during the vitrification process is linked with embryo phenotypic adaptation detected at adulthood. The phenotypic variation during the vitrification process may be associated with alterations in the genome methylation patterns in the liver tissue. Further research is needed to validate the significance of this finding.

5. References

Adamson, G.D., Mouzon, J., Chambers, G.M., Zegers-Hochschild, F., Mansour, R., Ishihara, O., Banker, M., Dyer, S. International committee for monitoring assisted reproductive technology: world report on assisted reproductive technology, 2011. Assisted reproduction. 2018. 110 (6): 1067-1079.

https://doi.org/10.1016/j.fertnstert.2018.06.039

Auroux, M., Cerutti, I., Ducot, B., Loeuillet, A. Is embryo-cryopreservation really neutral? A new long- term effect of embryo freezing in mice: protection of adults from induced cancer according to strain and sex. Reproduction Toxicology. 2004. 18: 813-818.

https://doi.org/10.1016/j.reprotox.2004.04.010

Besenfelder, U., Brem, G. Laparoscopic embryo transfer in rabbits. Journal of Reproduction and Fertility. 1993. 99: 53–56.

https://doi.org/10.1530/jrf.0.0990053

Blasco, A., Gómez, E. A note on growth curves of rabbit lines selected on growth rate or litter size. Anim. Prod. 1993. 57: 332–334,

https://doi.org/10.1017/S000335610000698X.

Calle, A., Miranda, A., Fernandez-Gonzalez, R., Pericuesta, E., Laguna, R., Gutierrez-Adan, A. Male mice produced by in vitro culture have reduced fertility and transmit organomegaly and glucose intolerance to their male offspring. Biology of reproduction. 2012. 87 (2): 34-43.

https://doi.org/10.1095/biolreprod.112.100743

Canovas, S., Ross, P.J., Kelsey, G., Coy, P. DNA methylation in embryo development: epigenetic impact of ART (Assisted Reproductive Technologies). BioEssays. 2017. 39 (11): 10.1002/bies.201700106.

https://doi.org/10.1002/bies.201700106

Charni-Natan, M., Aloni-Grinstein, R., Osher, E., Rotter, V. Liver and Steroid Hormones-Can a Touch of p53 Make a Difference?. Frontiers in endocrinology. 2019. 10: 374.

https://doi.org/10.3389/fendo.2019.00374

Chen, L., Yang, T., Zheng, Z., Yu, H., Wang, H., Qin, J. Birth prevalence of congenital malformations in singleton pregnancies resulting from in vitro fertilization/intracytoplasmic sperm injection worldwide: a systematic review and meta-analysis. Archives of gynecology and obstetrics. 2018. 297 (5): 1115–1130.

https://doi.org/10.1007/s00404-018-4712-x

Chen, L., Ni, X., Xu, Z., Fang, J., Zhang, N., Li, D. Effect of frozen and fresh embryo transfers on the birthweight of live-born twins. European journal of obstetrics, gynecology and reproductive Biology. 2020. 246: 50-54.

https://doi.org/10.1016/j.ejogrb.2020.01.008.

Chen, M., Heilbronn, L.K. The health outcomes of human offspring conceived by assisted reproductive technologies (ART). Journal of Developmental Origins of Health and Disease. 2017. 8: 388–402.

https://doi.org/10.1017/S2040174417000228

Chen, W., Peng, Y., Ma, X., Kong, S., Tang S., Wei, Y., Zhao, Y., Zhang, W., Wang, Y., Yan, L., Qiao, J. Epigenetic Effects of Assisted Reproductive Technology in Human Offspring. 2020. bioRxiv

https://doi.org/10.1101/816157

Conine, C.C., Krykbaeva, M., Song, L., Brewster, R.C., Friedman, N., Rando, O.J. Flexibility and constraint in preimplantation gene regulation in mouse. 2020. bioRxiv.

https://doi.org/10.1101/2020.03.13.990275

Donjacour, A., Liu, X., Lin, W., Simbulan, R., Rinaudo, P.F. In vitro fertilization affects growth and glucose metabolism in a sex-specific manner in an outbred mouse model. Biology of reproduction. 2014. 90 (4): 80.

https://doi.org/10.1095/biolreprod.113.113134

Dulioust, E., Toyama, K., Busnel, M.C., Moutier, R., Carlier, M., Marchaland, C., Ducot, B., Roubertoux, P., Auroux, M. Long-term effects of embryo freezing in mice. Proceedings of the National Academy of Sciences of the United States of America. 1995. 92 (2): 589–593.

https://doi.org/10.1073/pnas.92.2.589

Duranthon, V., Chavatte-Palmer, P. Long term effects of ART: What do animals tell us? Molecular reproduction and development. 2018. 85: 348-368.

https://doi.org/10.1002/mrd.22970

Ecker, D.J., Stein, P., Xu, Z., Williams, C.J., Kopf, G.S., Bilker, W.B., Abel, T., Schultz, R.M. Long-term effects of culture of preimplantation mouse embryos on behavior. Proceedings of the National Academy of Sciences of the United States of America. 2004. 101 (6): 1595–1600.

https://doi.org/10.1073/pnas.0306846101

Fauque, P., Mondon, F., Letourneur, F., Ripoche, M.A., Journot, L., Barbaux, S., Dandolo, L., Patrat, C., Wolf, J.P., Jouannet, P., Jammes, H., Vaiman, D. In vitro fertilization and embryo culture strongly impact the placental transcriptome in the mouse model. PloS one. 2010. 5 (2): e9218.

https://doi.org/10.1371/journal.pone.0009218

Fernández-Gonzalez, R., Moreira, P., Bilbao, A., Jiménez, A., Pérez-Crespo, M., Ramírez, M.A., Rodríguez De Fonseca, F., Pintado, B., Gutiérrez-Adán, A. Long-term effect of in vitro culture of mouse embryos with serum on mRNA expression of imprinting genes, development, and behavior. Proceedings of the National Academy of Sciences of the United States of America. 2004. 101 (16): 5880–5885.

https://doi.org/10.1073/pnas.0308560101

Fernandez-Gonzalez, R., Ramirez, M.A., Pericuesta, E., Calle, A., Gutierrez-Adan, A. Histone modifications at the blastocyst Axin1(Fu) locus mark the heritability of in vitro culture-induced epigenetic alterations in mice. Biology of reproduction. 2010. 83 (5): 720–727.

https://doi.org/10.1095/biolreprod.110.084715

Feuer, S.K., Donjacour, A., Simbulan, R.K., Lin, W., Liu, X., Maltepe, E., Rinaudo, P.F. Sexually dimorphic effect of in vitro fertilization (IVF) on adult mouse fat and liver metabolomes. Endocrinology. 2014. 155 (11): 4554–4567.

https://doi.org/10.1210/en.2014-1465

Feuer, S.K., Liu, X., Donjacour, A., Lin, W., Simbulan, R.K., Giritharan, G., Piane, L.D., Kolahi, K., Ameri, K., Maltepe, E., Rinaudo, P.F. Use of a mouse in vitro fertilization model to understand the developmental origins of health and disease hypothesis. Endocrinology. 2014. 155 (5): 1956–1969.

https://doi.org/10.1210/en.2013-2081

Feuer, S., Liu, X., Donjacour, A., Simbulan, R., Maltepe, E., Rinaudo, P. Transcriptional signatures throughout development: the effects of mouse embryo manipulation in vitro. Reproduction. 2017. 153 (1): 107-122.

https://doi.org/10.1530/REP-16-0473

Feuer, S.K., Rinaudo, P.F. Physiological, metabolic and transcriptional postnatal phenotypes of in vitro fertilization (IVF) in the mouse. Journal of Developmental Origins of Health and Disease. 2017. 8 (4): 403-410.

https://doi.org/10.1017/S204017441700023X

Feuer, S.K., Rinaudo, P.F. From embryos to adults: a DOHaD perspective on in vitro fertilization and other assisted reproductive technologies. Healthcare. 2016. 4 (3): 51-64.

https://doi.org/10.3390/healthcare4030051

Fleming, T.P., Velazquez, M.A., Eckert, J.J. Embryos, DOHaD and David Barker. Journal of developmental origins of health and disease. 2015. 6 (5): 377–383.

https://doi.org/10.1017/S2040174415001105

Franzago, M., Rovere, M.L., Franchi, P.G., Vitacolonna, E., Stuppia, L. Epigenetics and human reproduction: the primary prevention of the noncommunicable diseases. Epigenomics. 2019. 11 (12): 1441-1460.

https://doi.org/10.2217/epi-2019-0163

Garcia-Dominguez, X., Vicente, J.S., Marco-Jimenez, F. Developmental plasticity in response to embryo cryopreservation: the importance of the vitrification device in rabbits. Animals. 2020. 10 (5): E804.

https://doi.org/10.3390/ani10050804

Ghulam, M.M., Catala, M., Abou Elela, S. Differential expression of duplicated ribosomal protein genes modifies ribosome composition in response to stress. Nucleic Acids Research. 2020. 48 (4): 1954-1968.

https://doi.org/10.1093/nar/gkz1183

Goto, K., Mugurama, K., Kuramochi, T., Shimozawa, N., Hioki, K., Itoh, T., Ebukuro, M. Effects of cryopreservation of mouse embryos and in vitro fertilization on genotypic frequencies in colonies. Molecular reproduction and development. 2002. 62: 307-311.

https://doi.org/10.1002/mrd.10119

Green, M.P., Mouat, F., Miles, H.L., Hopkins, S.A., Derraik, J.G.B., Hofman, P.L., Peek, J.C., Cutfield, W.S. Phenotypic differences in children conceived from fresh and thawed embryos in in vitro fertilization compared with naturally conceived children. Fertility and Sterility. 2013. 99 (7): 1898-1904.

http://dx.doi.org/10.1016/j.fertnstert.2013.02.009

Gu, L., Zhang, J., Zheng, M., Dong, G., Xu, J., Zhang, W., Wu, Y., Yang, Y., Zhu, H. A potential high risk for fatty liver disease was found in mice generated after assisted reproductive techniques. Journal of cellular biochemistry. 2018. 119: 1899-1910.

https://doi.org/10.1002/jcb.26351

Guo, X.Y., Liu, X.M., Jin, L., Wang, T.T., Ullah, K., Sheng, J.Z., Huang, H.F. Cardiovascular and metabolic profiles of offspring conceived by assisted reproductive technologies: a systematic review and meta-analysis. Fertility and sterility. 2017. 107 (3): 622–631.

https://doi.org/10.1016/j.fertnstert.2016.12.007

Halliday, J., Lewis, S., Kennedy, J., Burgner, D.P., Juonala, M., Hammarberg, K., Amor, D.J., Doyle, L.W., Saffery, R., Ranganathan, S., Welsh, L., Cheung, M., McBain, J., Hearps, S., McLachlan, R. Health of adults aged 22 to 35 years conceived by assisted reproductive technology. Fertility and sterility. 2019. 112 (1): 130–139.

https://doi.org/10.1016/j.fertnstert.2019.03.001

Hiendleder, S., Wirtz, M., Mund, C., Klempt, M., Reichenbach, H., Stojkovic, M., Weppert, M., Wenigerkind, H., Elmlinger, M., Lyko, F., Schmitz, O.J., Wolf, E. Tissue-specific effects of in vitro fertilization procedures on genomic cytosine methylation levels in overgrown and normal sized bovine fetuses. Biology of reproduction. 2006. 75: 17-23.

https://doi.org/10.1095/biolreprod.105.043919

Hutanu, D., Bechir, M., Popescu, R. Epigenetics, assisted reproduction, and intracytoplasmic sperm injection: a review of the current data. European medical journal. 2019. 4 (2): 36-42.

Ivanova, E., Canovas, S., Garcia-Martínez, S., Romar, R., Lopes, J.S., Rizos, D., Sanchez-Calabuig, M.J., Krueger, F., Andrews S., Perez-Sanz, F., Kelsey, G., Coy, P. DNA methylation changes during preimplantation development reveal inter-species differences and reprogramming events at imprinted genes. Clinical Epigenetics. 2020. 12: 64.

https://doi.org/10.1186/s13148-020-00857-x

John, R.M, Rougeulle, C. Developmental epigenetics: phenotype and the flexible epigenome. Frontiers in cell and developmental biology. 2018. 6: 130.

https://doi.org/10.3389/fcell.2018.00130

Kilborn, S.H., Trudel, G., Uhthoff, H. Review of growth plate closure compared with age at sexual maturity and lifespan in laboratory animals. Contemporany topics in laboratory animal science. 2002. 41: 21-26

Kindsfather, A.J., Czekalski, M.A., Pressimone, C.A., Erisman, M.P., Mann, M.R. Perturbations in imprinted methylation from assisted reproductive technologies

but not advanced maternal age in mouse preimplantation embryos. Clinical epigenetics. 2019. 11 (1): 162.

https://doi.org/10.1186/s13148-019-0751-9

Kohda, T. Effects of embryonic manipulation and epigenetics. Journal of human genetics. 2013. 58 (7): 416–420.

https://doi.org/10.1038/jhg.2013.61

Kohda, T., Ishino, F. Embryo manipulation via assisted reproductive technology and epigenetic asymmetry in mammalian early development. Philosophical Transactions of the Royal Society B: Biological Sciences. 2013. 368 (1609).

https://doi.org/10.1098/rstb.2012.0353

La Rovere, M., Franzago, M., Stuppia, L. Epigenetics and Neurological Disorders in ART. International journal of molecular sciences. 2019. 20 (17): 4169.

https://doi.org/10.3390/ijms20174169

Lacagnina, S. The Developmental Origins of Health and Disease (DOHaD). American journal of lifestyle medicine. 2019. 14 (1): 47–50.

https://doi.org/10.1177/1559827619879694

Lavara, R., Baselga, M., Marco-Jiménez, F., Vicente, J.S. Long-term and transgenerational effects of cryopreservation on rabbit embryos. Theriogenology. 2014. 81: 988–992.

https://doi.org/10.1016/j.theriogenology.2014.01.030

Lavara, R., Baselga, M., Marco-Jiménez, F., Vicente, J.S. Embryo vitrification in rabbits: Consequences for progeny growth. Theriogenology. 2015. 84 (5): 674–680.

https://doi.org/10.1016/j.theriogenology.2015.04.025

Leese, H.J. Quiet Please, Do Not Disturb: A Hypothesis of Embryo Metabolism and Viability. Bioessays. 2002. 24: 845-9.

https://doi.10.1002/bies.10137.

Leese, H.J., Guerif, F., Allgar, V., Brison, D.R., Lundin, K., Sturmey, R.G. Biological optimization, the Goldilocks principle, and how much is lagom in the preimplantation embryo. Molecular reproduction and development. 2016. 83 (9): 748–754.

https://doi.org/10.1002/mrd.22684

Li, B., Xiao, X., Chen, S., Huang, J., Ma, Y., Tang, N., Sun, H., Wang, X. Changes of phospholipids in fetal liver of mice conceived by in vitro fertilization. Biology of reproduction. 2016. 94 (5): 1-8.

https://doi.org/10.1095/biolreprod.115.136325

Lienhard, M., Grimm, C., Morkel, M., Herwig, R., Chavez, L. MEDIPS: genome-wide differential coverage analysis of sequencing data derived from DNA enrichment exper-iments. Bioinformatics. 2014. 30: 284-286.

https://doi.org/10.1093/bioinformatics/btt650

Mani, S., Ghosh, J., Coutifaris, C., Sapienza, C., Mainigi, M. Epigenetic changes and assisted reproductive technologies. Epigenetics. 2020. 15 (1-2): 12-25.

https://doi.org/10.1080/15592294.2019.1646572

Marchesi, D.E., Qiao, J., Feng, H.L. Embryo manipulation and imprinting. Seminars in Reproductive Medicine. 2012. 30: 323–333.

https://doi.org/10.1055/s-0032-1320013

Marco-Jiménez, F., Lavara, R., Jiménez-Trigos, E., Vicente, J.S. In vivo development of vitrified rabbit embryos: effects of vitrification device, recipient genotype, and asynchrony. Theriogenology. 2013. 79 (7): 1124-1129.

https://doi.org/10.1016/j.theriogenology.2013.02.008

Marco-Jiménez, F., Baselga, M., Vicente, J.S. Successful re-establishment of a rabbit population from embryos vitrified 15 years ago: The importance of biobanks in livestock conservation. PLoS One. 2018. 13 (6): e0199234.

https://doi.org/10.1371/journal.pone.0199234

Marsico, T.V., de Camargo, J., Valente, R.S., Sudano, M.J. Embryo competence and cryosurvival: Molecular and cellular features. Animal Reproduction. 2019. 16: 423-439.

http://dx.doi.org/10.21451/1984-3143-AR2019-0072

Melamed, N., Choufani, S., Wilkins-Haug, L.E., Koren, G., Weksberg, R. Comparison of genome-wide and gene-specific DNA methylation between ART and naturally conceived pregnancies. Epigenetics. 2015. 10 (6): 474-483.

http://dx.doi.org/10.4161/15592294.2014.988041

Metsalu T, Vilo J. ClustVis: a web tool for visualizing clustering of multivariate data using Principal Component Analysis and heatmap. Nucleic Acids Res. 2015. 43: W566-70.

https://doi.org/10.1093/nar/gkv468

Nusbaumer, D., Da Cunha, L.M., Wedekind, C. Sperm cryopreservation reduces offspring growth. Proceedings of the Royal Society B Biological Science. 2019. 286: 1644.

https://doi.org/10.1098/rspb.2019.1644

Novakovic, B., Lewis, S., Halliday, J., Kennedy, J., Burgner, D.P., Czajko, A., Kim, B., Sexton-Oates, A., Juonala, M., Hammarberg, K., Amor, D.J., Doyle, L.W., Ranganathan, S., Welsh, L., Cheung, M., McBain, J., McLachlan, R., Saffery, R. Assisted reproductive technologies are associated with limited epigenetic variation at birth that largely resolves by adulthood. Nature. 2019. 10: 3922

https://doi.org/10.1038/s41467-019-11929-9

Ortiz-Rodriguez, J.M., Ortega-Ferrusola, C., Gil, M.C., Martín-Cano, F.E., Gaitskell-Phillips, G., Rodríguez-Martínez, H., Hinrichs, K., Álvarez-Barrientos, A., Román, Á., Peña, F.J. Transcriptome analysis reveals that fertilization with cryopreserved sperm downregulates genes relevant for early embryo development in the horse. PloS one. 2019. 14 (6): e0213420.

https://doi.org/10.1371/journal.pone.0213420

Ramos-Ibeas, P., Heras, S., Gómez-Redondo, I., Planells, B., Fernández-González, R., Pericuesta, E., Laguna-Barraza, R., Perez-Cerezales, S., Gutiérrez-Adán, A. Embryo responses to stress induced by assisted reproductive technologies. Molecular reproduction and development. 2019. 86 (10): 1292-1306.

https://doi.org/10.1002/mrd.23119

Robinson, M.D., McCarthy, D.J., Smyth, G.K. edgeR: a Bioconductor package for differential expression analysis of digital gene expression data. Bioinformatics. 2010. 26: 139-140.

https://doi.org/10.1093/bioinformatics/btp616

Roseboom, T.J. Developmental plasticity and its relevance to assisted human reproduction. Human reproduction. 2018. 33 (4): 546-552

https://doi.org/10.1093/humrep/dey034

Saenz-de-Juano, M.D., Marco-Jiménez, F., Schmaltz-Panneau, B., Jiménez-Trigos, E., Viudes-de-Castro, M.P., Peñaranda, D.S., Jouneau. L., Lecardonnel, J., Lavara, R., Naturil-Alfonso, C., Duranthon, V., Vicente, J.S. Vitrification alters rabbit foetal placenta at transcriptomic and proteomic level. Reproduction. 2014. 147 (6): 789-801.

https://doi.org/10.1530/REP-14-0019

Saenz-de-Juano, M.D., Marco-Jimenez, F., Viudes-de-Castro, M.P., Lavara, R., Vicente, J.S. Direct comparison of the effects of slow freezing and vitrification on late blastocyst gene expression, development, implantation and offspring of rabbit morulae. Reproduction in domestic animals = Zuchthygiene. 2014. 49 (3): 505–511.

https://doi.org/10.1111/rda.12320

Saenz-de-Juano, M.D., Vicente, J.S., Hollung, K., Marco-Jiménez, F. Effect of Embryo Vitrification on Rabbit Foetal Placenta Proteome during Pregnancy. PloS one. 2015. 10 (4): e0125157.

https://doi.org/10.1371/journal.pone.0125157

Schieve, L.A., Meikle, S.F., Ferre, C., Peterson, H.B., Jeng, G., Wilcox, L.S. Low and very low birth weight in infants conceived with use of assisted reproductive technology. New England journal of medicine. 2002. 346 (10): 731-737.

https://doi.org/10.1056/NEJMoa010806

Shaw, L., Sneddon, S.F., Brison, D.R., Kimber, S.J. Comparison of gene expression in fresh and frozen-thawed human preimplantation embryos. Reproduction. 2012.144 (5): 569-582.

https://doi.org/10.1530/REP-12-0047

Sirard, M.A. The influence of in vitro fertilization and embryo culture on the embryo epigenetic constituents and the possible consequences in the bovine model. 2017. 8 (4): 411-417.

https://doi.org/10.1017/S2040174417000125

Spijkers, S., Lens, J.W., Schats, R., Lambalk, C.B. Fresh and Frozen-Thawed Embryo Transfer Compared to Natural Conception: Differences in Perinatal Outcome. Gynecologic and obstetric investigation. 2017. 82 (6): 538-546.

https://doi.org/10.1159/000468935

Steptoea, P.C., Edwards, R.G. Birth after the reimplantation of a human embryo. The lancet. 1978. 312 (8085): 366.

https://doi.org/10.1016/S0140-6736(78)92957-4

Stout, T. Clinical insights: Assisted reproductive technologies. Equine Veterinary Journal. 2019. 51: 427–428.

https://doi.org/10.1111/evj.13099

Tachataki, M., Winston, R., Taylor, D. Quantitative RT±PCR reveals tuberous sclerosis gene, TSC2, mRNA degradation following cryopreservation in the human preimplantation embryo. Molecular human reproduction. 2003. 9 (10): 593-601.

https://doi.org/10.1093/molehr/gag073

Urrego, R., Rodriguez-Osorio, N., Heiner Niemann, H. Epigenetic disorders and altered gene expression after use of Assisted Reproductive Technologies in domestic cattle. Epigenetics. 2014. 9 (6): 803-815.

https://doi.org/10.4161/epi.2871

Velazquez, M.A., Sheth, B., Smith, S.J., Eckert, J.J., Osmond, C., Fleming, T.P. Insulin and branched-chain amino acid depletion during mouse preimplantation embryo culture programmes body weight gain and raised blood pressure during early postnatal life. Biochimica et biophysica acta. Molecular basis of disease. 2018. 1864 (2): 590–600.

https://doi.org/10.1016/j.bbadis.2017.11.020

Viana, C. 2018 Statistics of embryo production and transfer in domestic farm animals. Embryo Technology Newsletter. 2019. 36 (4).

Vicente, J.S., Viudes-de-Castro, M.P., García, M.L. In vivo survival rate of rabbit morulae after vitrification in a medium without serum protein. Reproduction, Nutrition, Development. 1999. 39: 657–662.

https://doi.org/10.1051/rnd:19990511

Vicente, J.S., Saenz-de-Juano, M.D., Jiménez-Trigos, E., Viudes-de-Castro, M.P., Peñaranda, D.S., Marco-Jiménez, F. Rabbit morula vitrification reduces early foetal growth and increases losses throughout gestation. Cryobiology. 2013. 67 (3): 321-326.

https://doi.org/10.1016/j.cryobiol.2013.09.165

Vidal, M., Vellvé, K., González-Comadran, M., Robles, A., Prat, M., Torné, M., Carreras, R., Checa, M.A. Perinatal outcomes in children born after fresh or frozen embryo transfer: a Catalan cohort study based on 14,262 newborns. Fertil Steril. 2017. 107 (4): 940-947.

https://doi.org/10.1016/j.fertnstert.2017.01.021

Vrooman, L.A., Bartolomei, M.S. Can assisted reproductive technologies cause adult-onset disease? Evidence from human and mouse. Reproductive toxicology. 2017. 68: 72-84.

https://doi.org/10.1016/j.reprotox.2016.07.015

Waal, E., Vrooman, L.A., Fischer, E., Ord, T., Mainigi, M.A., Coutifaris, C., Schultz, R.M., Bartolomei, M.S. The cumulative effect of assisted reproduction procedures on placental development and epigenetic perturbations in a mouse model. Human Molecular Genetics. 2015. 24 (24): 6975–6985.

https://doi.org/10.1093/hmg/ddv400

Wang, L.Y., Le, F., Wang, N., Li, L., Liu, X.Z., Zheng, Y.M., Lou, H.Y., Xu, X.R., Chen, Y.L., Zhu, X.M., Huang, H.F., Jin, F. Alteration of fatty acid metabolism in the liver, adipose tissue, and testis of male mice conceived through assisted reproductive technologies: fatty acid metabolism in ART mice. Lipids in health and disease. 2013. 12 (1): 5.

https://doi.org/10.1186/1476-511X-12-5

Wang, N., Li, C.Y., Zhu, H.B., Hao, H.S., Wang, H.Y., Yan, C.L., Zhao, S.J., Du, W.H., Wang, D., Liu, Y., Pang, Y.W., Zhao, X.M. Effect of vitrification on the mRNA transcriptome of bovine oocytes. Reproduction in domestic animals. 2017. 52 (4): 531–541.

https://doi.org/10.1111/rda.12942

Wang, Y.E., Kutnetsov, L., Partensky, A., Farid, J., Quackenbush, J. WebMeV: a cloud platform for analyzing and visualizing cancer genomic data. Cancer research. 2017. 77: e11-e14.

https://doi.org/10.1158/0008-5472.CAN-17-0802.

Windisch, H.S., Frickenhaus, S., John, U., Knust, R., Pörtner, H.O., Lucassen, M. Stress response or beneficial temperature acclimation: transcriptomic signatures in Antarctic fish (Pachycara brachycephalum). Molecular ecology. 2014. 23 (14): 3469-3482.

https://doi.org/10.1111/mec.12822

Winick, M., Noble, A. Quantitative changes in DNA, RNA, and protein during prenatal and postnatal growth in the rat. Developmental biology. 1965. 12 (3): 451–466.

https://doi.org/10.1016/0012-1606(65)90009-6

Wong, K.M., Mastenbroek, S., Repping, S. Cryopreservation of human embryos and its contribution to in vitro fertilization success rates. Fertility and sterility. 2014. 102 (1): 19-26.

https://doi.org/10.1016/j.fertnstert.2014.05.027

Zandstra, H., Brentjens, L., Spauwen, B., Touwslager, R., Bons, J., Mulder, A.L., Smits, L., van der Hoeven, M., van Golde, R., Evers, J., Dumoulin, J., Van Montfoort, A. Association of culture medium with growth, weight and cardiovascular development of IVF children at the age of 9 years. Human reproduction. 2018. 33 (9): 1645–1656.

https://doi.org/10.1093/humrep/dey246

Zhang, W.Y., Selamet Tierney, E.S., Chen, A.C., Ling, A.Y., Fleischmann, R.R., Baker, V.L. Vascular Health of Children Conceived via In Vitro Fertilization. The Journal of paediatrics. 2019. 214: 47–53.

https://doi.org/10.1016/j.jpeds.2019.07.033

6. Annexed

Suplementary data 1. Differentially methylated genes of F0 in liver tissue due to effect of the embryo vitrification-transfer procedure.

Type	Gene_ID	Gene_name	Δβ
Hypo	108177783	transfer RNA aspartic acid (anticodon GUC)(TRNAD-GUC)	-43,34
Hypo	108177773	transfer RNA glycine (anticodon UCC)(TRNAG-UCC)	-30,48
Hypo	108177782	transfer RNA glycine (anticodon UCC)(TRNAG-UCC)	-27,47
Hypo	108177834	transfer RNA leucine (anticodon CAG)(TRNAL-CAG)	-26,21
Hypo	108177792	transfer RNA glycine (anticodon UCC)(TRNAG-UCC)	-24,38
Hypo	108177775	transfer RNA glutamic acid (anticodon CUC)(TRNAE-CUC)	-24,07
Hypo	108177774	transfer RNA aspartic acid (anticodon GUC)(TRNAD-GUC)	-22,40
Hypo	108177860	transfer RNA leucine (anticodon CAG)(TRNAL-CAG)	-17,93
Hypo	108177772	transfer RNA glutamic acid (anticodon CUC)(TRNAE-CUC)	-16,25
Hypo	108176087	TBC1 domain family member 3B-like(LOC108176087)	-15,92
Hypo	103348417	homeobox protein prophet of Pit-1-like(LOC103348417)	-15,59
Hypo	108177791	transfer RNA glutamic acid (anticodon CUC)(TRNAE-CUC)	-12,79
Hypo	100338734	kelch-like protein 26(LOC100338734)	-12,48
Hypo	100340624	adenomatous polyposis coli protein 2 pseudogene(LOC100340624)	-9,81
Hypo	103347403	E3 ubiquitin-protein ligase RNF213 pseudogene(LOC103347403)	-8,95
Hypo	103347157	DENN domain-containing protein 3-like(LOC103347157)	-8,55
Hypo	108177785	transfer RNA glycine (anticodon UCC)(TRNAG-UCC)	-8,50
Hypo	100125980	cAMP-dependent protein kinase type I-beta regulatory subunit(LOC100125980)	-8,14
Hypo	103346914	adenomatous polyposis coli protein 2 pseudogene(LOC103346914)	-7,92
Hypo	100339787	40S ribosomal protein S28(LOC100339787)	-7,66
Hypo	100343629	mediator complex subunit 25(MED25)	-7,57
Hypo	103346776	CDC42 binding protein kinase gamma(CDC42BPG)	-7,50
Hypo	103346570	splicing factor, arginine/serine-rich 19(LOC103346570)	-7,33
Hypo	100347128	tubulin polyglutamylase complex subunit 1(TPGS1)	-7,15
Hypo	100345364	basic helix-loop-helix family member a9(BHLHA9)	-6,97
Hypo	103345318	proline-serine-threonine phosphatase interacting protein 1(PSTPIP1)	-6,92
Hypo	103346850	Fanconi anemia core complex-associated protein 100(LOC103346850)	-6,84

Type	Gene_ID	Gene_name	Δβ
Hypo	100348201	THAP domain containing 7(THAP7)	-6,54
Hypo	100337872	leucine rich repeats and WD repeat domain containing 1(LRWD1)	-6,01
Hypo	103347551	coiled-coil domain containing 61(CCDC61)	-5,93
Hypo	103347625	uncharacterized LOC103347625(LOC103347625)	-5,78
Hypo	100340044	nephrocystin 4(NPHP4)	-5,74
Hypo	103347482	multiple epidermal growth factor-like domains protein 6 pseudogene(LOC103347482)	-5,72
Hypo	103346997	BLOC-1 related complex subunit 8(BORCS8)	-5,69
Hypo	103346452	TBC1 domain family member 26(LOC103346452)	-5,69
Hypo	108175884	purinergic receptor P2Y11(P2RY11)	-5,47
Hypo	100342868	nuclear receptor subfamily 1 group H member 2(NR1H2)	-5,42
Hypo	103346879	glutenin, high molecular weight subunit PW212-like(LOC103346879)	-5,42
Hypo	100352732	forkhead box protein K1 pseudogene(LOC100352732)	-5,06
Hypo	103347612	homeobox protein CDX-2-like(LOC103347612)	-4,96
Hypo	103346214	collagen alpha-1(I) chain-like(LOC103346214)	-4,90
Hypo	100347957	ERCC excision repair 2, TFIIH core complex helicase subunit(ERCC2)	-4,88
Hypo	103347251	zinc finger protein 579(ZNF579)	-4,85
Hypo	108176314	acid phosphatase, testicular(ACPT)	-4,78
Hypo	103347222	family with sequence similarity 83 member H(FAM83H)	-4,56
Hypo	100347607	WD repeat-containing protein 46 pseudogene(LOC100347607)	-4,51
Hypo	103346847	NLR family pyrin domain containing 6(NLRP6)	-4,39
Hypo	100350842	transmembrane protein 88(TMEM88)	-4,36
Hypo	103351074	uncharacterized LOC103351074(LOC103351074)	-4,21
Hypo	100353245	interferon-induced transmembrane protein 3-like(LOC100353245)	-4,16
Hypo	103345186	uncharacterized LOC103345186(LOC103345186)	-4,11
Hypo	100355673	tigger transposable element derived 3(TIGD3)	-4,02
Hypo	100338383	coiled-coil domain containing 166(CCDC166)	-3,97
Hypo	100009035	histamine receptor H3(HRH3)	-3,85
Hypo	103346269	EF-hand calcium-binding domain-containing protein 6(LOC103346269)	-3,84
Hypo	108178781	uncharacterized LOC108178781(LOC108178781)	-3,81
Hypo	100350203	peptidyl-tRNA hydrolase 1 homolog(PTRH1)	-3,77
Hypo	100349704	60S ribosomal protein L29 pseudogene(LOC100349704)	-3,67

Type	Gene_ID	Gene_name	Δβ
Hypo	100348531	solute carrier family 25 member 34(SLC25A34)	-3,67
Hypo	103346260	zinc finger BED-type containing 3(ZBED3)	-3,55
Hypo	108175975	formin-like protein 20(LOC108175975)	-3,51
Hypo	100342104	proline rich 5(PRR5)	-3,40
Hypo	100341880	dolichyl-diphosphooligosaccharide--protein glycosyltransferase non-catalytic subunit(DDOST)	-3,39
Hypo	103346306	kinesin light chain 3(KLC3)	-3,39
Hypo	103351573	polymerase I and transcript release factor(PTRF)	-3,29
Hypo	108178665	uncharacterized LOC108178665(LOC108178665)	-3,19
Hypo	103346453	E3 ubiquitin-protein ligase UHRF2 pseudogene(LOC103346453)	-3,19
Hypo	100342106	chromosome unknown open reading frame, human C19orf53(LOC100342106)	-3,17
Hypo	103345045	G protein-coupled receptor kinase 2(GRK2)	-3,13
Hypo	103346296	patatin-like phospholipase domain-containing protein 3(LOC103346296)	-3,11
Hypo	100355241	exocyst complex component 3 like 4(EXOC3L4)	-3,05
Hypo	100352445	40S ribosomal protein S2 pseudogene(LOC100352445)	-2,98
Hypo	100343627	heterogeneous nuclear ribonucleoprotein A1 pseudogene(LOC100343627)	-2,94
Hypo	100343858	family with sequence similarity 32 member A(FAM32A)	-2,94
Hypo	100340065	N-acetyltransferase 6(NAT6)	-2,94
Hypo	108176338	transfer RNA glycine (anticodon UCC)(TRNAG-UCC)	-2,93
Hypo	100354504	ISG15 ubiquitin-like modifier(ISG15)	-2,93
Hypo	100354386	HUS1 checkpoint clamp component B(HUS1B)	-2,91
Hypo	100358400	branched chain amino acid transaminase 2(BCAT2)	-2,90
Hypo	100351378	ER membrane protein complex subunit 8(EMC8)	-2,90
Hypo	103346777	menin 1(MEN1)	-2,83
Hypo	100144330	C-C motif chemokine receptor 10(CCR10)	-2,78
Hypo	100357032	Cbl proto-oncogene C(CBLC)	-2,76
Hypo	100346044	solute carrier family 18 member A3(SLC18A3)	-2,68
Hypo	103347553	sarcosine dehydrogenase, mitochondrial(LOC103347553)	-2,66
Hypo	100356845	mesoderm development candidate 1(MESDC1)	-2,66
Hypo	100352723	transmembrane protein 160(TMEM160)	-2,62
Hypo	100346763	UPF0235 protein C15orf40 homolog pseudogene(LOC100346763)	-2,59

Type	Gene_ID	Gene_name	Δβ
Hypo	103347187	solute carrier family 39 member 4(SLC39A4)	-2,58
Hypo	100338886	maestro heat like repeat family member 6(MROH6)	-2,55
Hypo	103346995	regulatory factor X associated ankyrin containing protein(RFXANK)	-2,45
Hypo	103346309	F-box only protein 46(LOC103346309)	-2,42
Hypo	100357510	G protein-coupled receptor 25(GPR25)	-2,40
Hypo	100337756	heat shock protein HSP 90-beta pseudogene(LOC100337756)	-2,39
Hypo	100344043	soluble scavenger receptor cysteine-rich domain-containing protein SSC5D(LOC100344043)	-2,39
Hypo	103349197	uncharacterized LOC103349197(LOC103349197)	-2,39
Hypo	100343532	keratin-associated protein 10-7-like(LOC100343532)	-2,39
Hypo	100341329	ovo like transcriptional repressor 1(OVOL1)	-2,38
Hypo	103352097	uncharacterized LOC103352097(LOC103352097)	-2,35
Hypo	100350561	multiple inositol polyphosphate phosphatase 1-like(LOC100350561)	-2,31
Hypo	808223	NADH dehydrogenase subunit 6(ND6)	-2,26
Hypo	100345914	guanylate kinase pseudogene(LOC100345914)	-2,24
Hypo	100343255	cytochrome c oxidase subunit 8A, mitochondrial(LOC100343255)	-2,22
Hypo	100359189	chromobox 4(CBX4)	-2,15
Hypo	100343111	leukocyte immunoglobulin-like receptor subfamily A member 5(LOC100343111)	-2,15
Hypo	808227	cytochrome b(CYTB)	-2,14
Hypo	100357290	caseinolytic mitochondrial matrix peptidase proteolytic subunit(CLPP)	-2,13
Hypo	100338584	ras-related protein Rap-1b pseudogene(LOC100338584)	-2,13
Hypo	108175487	uncharacterized LOC108175487(LOC108175487)	-2,07
Hypo	100347459	small nuclear ribonucleoprotein D2 polypeptide(SNRPD2)	-2,02
Hypo	808222	NADH dehydrogenase subunit 4L(ND4L)	-2,00
Hypo	103348739	39S ribosomal protein L20, mitochondrial(LOC103348739)	-2,00
Hypo	100353896	olfactory receptor 2L3-like(LOC100353896)	-1,99
Hypo	100353156	protocadherin beta-14(LOC100353156)	-1,98
Hypo	108178223	prosaposin receptor GPR37L1-like(LOC108178223)	-1,97
Hypo	100351483	H/ACA ribonucleoprotein complex subunit 2 pseudogene(LOC100351483)	-1,93
Hypo	100355350	erythropoietin receptor(EPOR)	-1,93
Hypo	100354993	trafficking protein particle complex 5(TRAPPC5)	-1,93

Type	Gene_ID	Gene_name	Δβ
Hypo	103351756	hepatocyte nuclear factor 1-alpha pseudogene(LOC103351756)	-1,92
Hypo	100344259	stromal cell derived factor 2 like 1(SDF2L1)	-1,87
Hypo	108176180	uncharacterized LOC108176180(LOC108176180)	-1,87
Hypo	100346259	von Willebrand factor A domain containing 1(VWA1)	-1,86
Hypo	100355682	phosphoenolpyruvate carboxykinase 1(PCK1)	-1,86
Hypo	100354658	mitochondrial ribosomal protein L49(MRPL49)	-1,86
Hypo	100342181	exosome component 4(EXOSC4)	-1,84
Hypo	100357035	alkB homolog 7(ALKBH7)	-1,80
Hypo	100353758	SWI/SNF-related matrix-associated actin-dependent regulator of chromatin subfamily E member 1 pseudogene(LOC100353758)	-1,79
Hypo	108175985	uncharacterized LOC108175985(LOC108175985)	-1,75
Hypo	100349214	adrenomedullin 2(ADM2)	-1,75
Hypo	103346569	splicing factor, arginine/serine-rich 19(LOC103346569)	-1,75
Hypo	100339128	solute carrier family 16 member 3(SLC16A3)	-1,73
Hypo	100353495	adenomatous polyposis coli protein 2-like(LOC100353495)	-1,71
Hypo	100357182	dCTP pyrophosphatase 1(DCTPP1)	-1,69
Hypo	103348617	transmembrane protein 120A(TMEM120A)	-1,67
Hypo	808221	NADH dehydrogenase subunit 3(ND3)	-1,67
Hypo	108176051	MAP/microtubule affinity-regulating kinase 4 pseudogene(LOC108176051)	-1,67
Hypo	100349309	RAB26, member RAS oncogene family(RAB26)	-1,66
Hypo	100356260	B-cell CLL/lymphoma 3(BCL3)	-1,66
Hypo	100348457	CD3e molecule associated protein(CD3EAP)	-1,65
Hypo	100338536	C1q and tumor necrosis factor related protein 5(C1QTNF5)	-1,64
Hypo	100354151	retinal rod rhodopsin-sensitive cGMP 3',5'-cyclic phosphodiesterase subunit delta pseudogene(LOC100354151)	-1,64
Hypo	100341971	Rab interacting lysosomal protein(RILP)	-1,63
Hypo	100343096	small nuclear ribonucleoprotein-associated protein B pseudogene(LOC100343096)	-1,59
Hypo	108176063	formin-like protein 5(LOC108176063)	-1,56
Hypo	100348172	pyruvate kinase PKM pseudogene(LOC100348172)	-1,53
Hypo	808224	NADH dehydrogenase subunit 5(ND5)	-1,53
Hypo	100337842	creatine kinase B-type pseudogene(LOC100337842)	-1,52
Hypo	103346308	F-box protein 46(FBXO46)	-1,50

Type	Gene_ID	Gene_name	Δβ
Hypo	808233	cytochrome c oxidase subunit II(COX2)	-1,48
Hypo	100342765	leucine rich repeat containing 3(LRRC3)	-1,46
Hypo	103347541	cleft lip and palate transmembrane protein 1-like protein(LOC103347541)	-1,44
Hypo	103346994	nuclear receptor 2C2 associated protein(NR2C2AP)	-1,43
Hypo	103345298	uncharacterized LOC103345298(LOC103345298)	-1,41
Hypo	100009282	eukaryotic translation elongation factor 1 gamma(EEF1G)	-1,40
Hypo	108176059	uncharacterized LOC108176059(LOC108176059)	-1,40
Hypo	100359278	sugar transporter SWEET1 pseudogene(LOC100359278)	-1,36
Hypo	103346448	ras GTPase-activating protein 4B-like(LOC103346448)	-1,33
Hypo	100357853	coiled-coil domain containing 185(CCDC185)	-1,33
Hypo	100349817	insulin like growth factor binding protein 1(IGFBP1)	-1,32
Hypo	100348713	ERCC excision repair 1, endonuclease non-catalytic subunit(ERCC1)	-1,31
Hypo	103347536	1-phosphatidylinositol 4,5-bisphosphate phosphodiesterase beta-3-like(LOC103347536)	-1,29
Hypo	100354254	cytochrome c oxidase subunit 8B, mitochondrial-like(LOC100354254)	-1,29
Hypo	108175798	uncharacterized LOC108175798(LOC108175798)	-1,28
Hypo	100343458	mercaptopyruvate sulfurtransferase(MPST)	-1,27
Hypo	103352511	natriuretic peptide B(NPPB)	-1,27
Hypo	808225	NADH dehydrogenase subunit 4(ND4)	-1,27
Hypo	808230	NADH dehydrogenase subunit 2(ND2)	-1,26
Hypo	100358214	taste 2 receptor member 38(TAS2R38)	-1,25
Hypo	103347461	Ig heavy chain V-A2 region P-MU-3-like(LOC103347461)	-1,24
Hypo	808229	cytochrome c oxidase subunit III(COX3)	-1,23
Hypo	100349530	Sp6 transcription factor(SP6)	-1,23
Hypo	108176334	transfer RNA leucine (anticodon CAG)(TRNAL-CAG)	-1,22
Hypo	103347114	LSM4 homolog, U6 small nuclear RNA and mRNA degradation associated(LSM4)	-1,22
Hypo	103347291	uncharacterized LOC103347291(LOC103347291)	-1,21
Hypo	108175375	SNRPN upstream reading frame protein(LOC108175375)	-1,20
Hypo	100340865	polyadenylate-binding protein 1 pseudogene(LOC100340865)	-1,19
Hypo	100355909	dynamin 1(DNM1)	-1,16
Hypo	100351218	claudin 5(CLDN5)	-1,16

Type	Gene_ID	Gene_name	Δβ
Hypo	100344692	carbonyl reductase [NADPH] 1(LOC100344692)	-1,15
Hypo	108177844	transfer RNA glycine (anticodon UCC)(TRNAG-UCC)	-1,15
Hypo	108177243	MAPK-interacting and spindle-stabilizing protein-like(LOC108177243)	-1,13
Hypo	100009337	apolipoprotein E(APOE)	-1,11
Hypo	100344799	kallikrein related peptidase 10(KLK10)	-1,10
Hypo	100341163	oxidative stress induced growth inhibitor 1(OSGIN1)	-1,10
Hypo	108175893	uncharacterized LOC108175893(LOC108175893)	-1,09
Hypo	108177658	small nuclear ribonucleoprotein G pseudogene(LOC108177658)	-1,09
Hypo	100348402	KH domain containing 3 like, subcortical maternal complex member(KHDC3L)	-1,08
Hypo	100356985	histone H3.3-like(LOC100356985)	-1,06
Hypo	100347432	solute carrier family 16 member 11(SLC16A11)	-1,06
Hypo	103346901	Ig heavy chain V-A1 region BS-5-like(LOC103346901)	-1,06
Hypo	108178652	immunoglobulin omega chain-like(LOC108178652)	-1,03
Hypo	103345144	uncharacterized LOC103345144(LOC103345144)	-1,03
Hypo	108175671	translation initiation factor IF-2-like(LOC108175671)	-1,03
Hypo	108177797	transfer RNA leucine (anticodon CAG)(TRNAL-CAG)	-1,03
Hypo	808226	NADH dehydrogenase subunit 1(ND1)	-1,00
Hypo	108177888	small nuclear ribonucleoprotein-associated protein B' pseudogene(LOC108177888)	-0,98
Hypo	100341919	AP-3 complex subunit sigma-1(LOC100341919)	-0,96
Hypo	100357198	zinc finger HIT-type containing 2(ZNHIT2)	-0,93
Hypo	108176769	transfer RNA glycine (anticodon GCC)(TRNAG-GCC)	-0,92
Hypo	100357329	cytochrome c(LOC100357329)	-0,90
Hypo	100352196	nuclease-sensitive element-binding protein 1 pseudogene(LOC100352196)	-0,88
Hypo	108176957	transfer RNA cysteine (anticodon GCA)(TRNAC-GCA)	-0,86
Hypo	808232	ATP synthase F0 subunit 6(ATP6)	-0,86
Hypo	100343034	ladybird homeobox 2(LBX2)	-0,85
Hypo	103349899	protein lin-28 homolog A pseudogene(LOC103349899)	-0,84
Hypo	100350792	10 kDa heat shock protein, mitochondrial pseudogene(LOC100350792)	-0,82
Hypo	108175776	docking protein 2 pseudogene(LOC108175776)	-0,81
Hypo	100358213	zymogen granule membrane protein 16-like(LOC100358213)	-0,76

Type	Gene_ID	Gene_name	Δβ
Hypo	108176736	uncharacterized LOC108176736(LOC108176736)	-0,76
Hypo	808228	ATP synthase F0 subunit 8(ATP8)	-0,74
Hypo	100353233	histone H1.0(LOC100353233)	-0,71
Hypo	100341000	OTU domain-containing protein 4-like(LOC100341000)	-0,66
Hypo	100352197	enhancer of rudimentary homolog(LOC100352197)	-0,64
Hypo	103345247	T-cell receptor beta chain V region CTL-L17-like(LOC103345247)	-0,57
Hypo	100356346	olfactory receptor 4X2-like(LOC100356346)	-0,56
Hypo	108176819	60S ribosomal protein L39-like(LOC108176819)	-0,49
Hyper	103345671	uncharacterized LOC103345671(LOC103345671)	0,37
Hyper	108175635	T-cell receptor beta chain V region CTL-L17-like(LOC108175635)	0,41
Hyper	100353390	interferon alpha-21-like(LOC100353390)	0,41
Hyper	100348557	nucleolar protein of 40 kDa pseudogene(LOC100348557)	0,46
Hyper	108178819	zinc finger protein 367-like(LOC108178819)	0,47
Hyper	100352257	prostaglandin E synthase 3 pseudogene(LOC100352257)	0,49
Hyper	108177194	transfer RNA lysine (anticodon CUU)(TRNAK-CUU)	0,52
Hyper	100356298	cyclin-dependent kinase 1 pseudogene(LOC100356298)	0,53
Hyper	100341428	60S ribosomal protein L11-like(LOC100341428)	0,55
Hyper	100347813	olfactory receptor-like protein OLF3(LOC100347813)	0,56
Hyper	100339454	40S ribosomal protein S27-like(LOC100339454)	0,56
Hyper	108175655	T-cell receptor beta chain V region CTL-L17-like(LOC108175655)	0,58
Hyper	100351519	L-lactate dehydrogenase A chain-like(LOC100351519)	0,58
Hyper	108176301	transfer RNA glycine (anticodon CCC)(TRNAG-CCC)	0,58
Hyper	100357515	olfactory receptor-like protein DTMT(LOC100357515)	0,62
Hyper	108175794	60S ribosomal protein L21(LOC108175794)	0,66
Hyper	108175777	40S ribosomal protein S24 pseudogene(LOC108175777)	0,67
Hyper	100352743	putative methyl-CpG-binding domain protein 3-like 3(LOC100352743)	0,69
Hyper	108176204	protein LSM12 homolog pseudogene(LOC108176204)	0,71
Hyper	100343251	40S ribosomal protein S6 pseudogene(LOC100343251)	0,71
Hyper	100342594	nucleoporin SEH1 pseudogene(LOC100342594)	0,72
Hyper	100354715	fumarate hydratase, mitochondrial-like(LOC100354715)	0,76
Hyper	100359303	tropomodulin-3(LOC100359303)	0,76
Hyper	103350978	uncharacterized LOC103350978(LOC103350978)	0,76

Type	Gene_ID	Gene_name	Δβ
Hyper	103351257	uncharacterized LOC103351257(LOC103351257)	0,82
Hyper	100359293	chloride intracellular channel protein 1 pseudogene(LOC100359293)	0,82
Hyper	100349168	proteasome inhibitor PI31 subunit pseudogene(LOC100349168)	0,83
Hyper	108177226	Ig lambda chain V-VI region EB4-like(LOC108177226)	0,83
Hyper	108177236	transfer RNA glycine (anticodon UCC)(TRNAG-UCC)	0,83
Hyper	100344064	elongation factor 1-alpha 1 pseudogene(LOC100344064)	0,84
Hyper	100348336	60S ribosomal protein L10-like(LOC100348336)	0,85
Hyper	100343325	S-phase kinase-associated protein 1 pseudogene(LOC100343325)	0,86
Hyper	100353168	protein FAM60A pseudogene(LOC100353168)	0,88
Hyper	103348819	cuticle collagen 40-like(LOC103348819)	0,91
Hyper	108177187	60S ribosomal protein L37 pseudogene(LOC108177187)	0,92
Hyper	108177009	40S ribosomal protein S27-like(LOC108177009)	0,92
Hyper	108176088	estradiol 17-beta-dehydrogenase 11 pseudogene(LOC108176088)	0,95
Hyper	100345710	COMM domain-containing protein 3 pseudogene(LOC100345710)	0,96
Hyper	108175434	leucine-rich repeat-containing protein 37A3-like(LOC108175434)	0,97
Hyper	100352363	cytochrome c oxidase subunit 6C(LOC100352363)	1,01
Hyper	100356530	olfactory receptor 14C36-like(LOC100356530)	1,03
Hyper	100356497	poly(rC)-binding protein 2-like(LOC100356497)	1,04
Hyper	100354397	interferon omega-1-like(LOC100354397)	1,04
Hyper	108176327	glycine cleavage system H protein, mitochondrial-like(LOC108176327)	1,05
Hyper	100353915	60S ribosomal protein L17 pseudogene(LOC100353915)	1,06
Hyper	100345190	ubiquitin-conjugating enzyme E2 L3(LOC100345190)	1,07
Hyper	108178019	60S ribosomal protein L21(LOC108178019)	1,09
Hyper	100358728	pre-mRNA-processing factor 17-like(LOC100358728)	1,10
Hyper	108175982	uncharacterized LOC108175982(LOC108175982)	1,10
Hyper	103349107	RNMT-activating mini protein pseudogene(LOC103349107)	1,11
Hyper	100347468	40S ribosomal protein S11(LOC100347468)	1,11
Hyper	108175630	T-cell receptor beta chain V region YT35-like(LOC108175630)	1,12
Hyper	103347513	stabilin-2(LOC103347513)	1,14
Hyper	108176576	60S ribosomal protein L39 pseudogene(LOC108176576)	1,16
Hyper	103349582	kelch repeat and BTB domain-containing protein 2-like(LOC103349582)	1,17
Hyper	100348375	olfactory receptor 2T29-like(LOC100348375)	1,17

Type	Gene_ID	Gene_name	Δβ
Hyper	108175641	T-cell receptor beta chain V region CTL-L17-like(LOC108175641)	1,17
Hyper	108176287	uncharacterized LOC108176287(LOC108176287)	1,18
Hyper	103350105	dihydrofolate reductase-like(LOC103350105)	1,19
Hyper	108177090	uncharacterized LOC108177090(LOC108177090)	1,20
Hyper	100354910	interferon omega-1-like(LOC100354910)	1,20
Hyper	100355833	WAS/WASL-interacting protein family member 2 pseudogene(LOC100355833)	1,21
Hyper	100338308	protein FAM136A pseudogene(LOC100338308)	1,22
Hyper	100351960	uncharacterized LOC100351960(LOC100351960)	1,23
Hyper	100341865	acyl-protein thioesterase 1-like(LOC100341865)	1,25
Hyper	100339396	THO complex subunit 7 homolog pseudogene(LOC100339396)	1,25
Hyper	103350719	uncharacterized LOC103350719(LOC103350719)	1,26
Hyper	108177287	60S ribosomal protein L23a pseudogene(LOC108177287)	1,26
Hyper	100353143	olfactory receptor 52H1-like(LOC100353143)	1,27
Hyper	100354440	40S ribosomal protein SA-like(LOC100354440)	1,28
Hyper	100344139	glucosamine 6-phosphate N-acetyltransferase pseudogene(LOC100344139)	1,29
Hyper	108178868	butyrophilin subfamily 2 member A2-like(LOC108178868)	1,30
Hyper	100349991	hsc70-interacting protein pseudogene(LOC100349991)	1,32
Hyper	100349737	group XIIA secretory phospholipase A2 pseudogene(LOC100349737)	1,33
Hyper	100354156	putative olfactory receptor 52P1(LOC100354156)	1,33
Hyper	100359071	mitochondrial carrier homolog 2 pseudogene(LOC100359071)	1,36
Hyper	108175634	T-cell receptor beta chain V region PHDS203-like(LOC108175634)	1,37
Hyper	100341134	spermine synthase pseudogene(LOC100341134)	1,38
Hyper	108178474	glycine cleavage system H protein, mitochondrial-like(LOC108178474)	1,38
Hyper	100350457	60S ribosomal protein L8 pseudogene(LOC100350457)	1,40
Hyper	100340083	40S ribosomal protein S23 pseudogene(LOC100340083)	1,43
Hyper	100340830	zinc finger CCHC-type and RNA-binding motif-containing protein 1(LOC100340830)	1,48
Hyper	108177856	transfer RNA glycine (anticodon CCC)(TRNAG-CCC)	1,49
Hyper	100342388	lysophosphatidylcholine acyltransferase 2B-like(LOC100342388)	1,49
Hyper	100353320	cytochrome c oxidase subunit 7B, mitochondrial(LOC100353320)	1,50
Hyper	108177112	60S ribosomal protein L23a pseudogene(LOC108177112)	1,51

Type	Gene_ID	Gene_name	Δβ
Hyper	100351957	60S ribosomal protein L6 pseudogene(LOC100351957)	1,53
Hyper	100352409	ADP/ATP translocase 2 pseudogene(LOC100352409)	1,54
Hyper	100343184	sugar transporter SWEET1 pseudogene(LOC100343184)	1,54
Hyper	100339296	uncharacterized LOC100339296(LOC100339296)	1,54
Hyper	108175636	T-cell receptor beta chain V region PHDS203-like(LOC108175636)	1,54
Hyper	100346036	60S ribosomal protein L9 pseudogene(LOC100346036)	1,55
Hyper	100351937	ribonuclease P/MRP subunit p38(RPP38)	1,61
Hyper	100344199	maspardin-like(LOC100344199)	1,62
Hyper	103351133	uncharacterized LOC103351133(LOC103351133)	1,64
Hyper	108177887	non-histone chromosomal protein HMG-17 pseudogene(LOC108177887)	1,65
Hyper	100008711	binder of sperm 1(BSP1)	1,66
Hyper	108178018	60S ribosomal protein L17 pseudogene(LOC108178018)	1,66
Hyper	108175654	T-cell receptor beta chain V region C5-like(LOC108175654)	1,69
Hyper	100339585	40S ribosomal protein SA pseudogene(LOC100339585)	1,70
Hyper	108177974	60S ribosomal protein L23a(LOC108177974)	1,72
Hyper	100347877	olfactory receptor 2T27-like(LOC100347877)	1,74
Hyper	100346519	60S ribosomal protein L32 pseudogene(LOC100346519)	1,76
Hyper	100345631	testis-expressed sequence 10 protein-like(LOC100345631)	1,79
Hyper	100357355	developmental pluripotency-associated protein 4 pseudogene(LOC100357355)	1,81
Hyper	100339330	E3 ubiquitin-protein ligase RNF138-like(LOC100339330)	1,81
Hyper	100343444	heterogeneous nuclear ribonucleoprotein A1-like(LOC100343444)	1,82
Hyper	100348244	pleckstrin homology domain-containing family B member 2 pseudogene(LOC100348244)	1,83
Hyper	103346478	leucine-rich repeat-containing protein 37A2(LOC103346478)	1,84
Hyper	100339620	olfactory receptor 2M3-like(LOC100339620)	1,87
Hyper	103352070	T-complex protein 1 subunit alpha pseudogene(LOC103352070)	1,88
Hyper	100345822	eukaryotic translation initiation factor 1A, X-chromosomal-like(LOC100345822)	1,92
Hyper	100355262	L-lactate dehydrogenase A chain-like(LOC100355262)	1,94
Hyper	100346271	zymogen granule membrane protein 16(LOC100346271)	1,99
Hyper	103346641	uncharacterized LOC103346641(LOC103346641)	2,00
Hyper	103346859	calcyclin-binding protein-like(LOC103346859)	2,01

Type	Gene_ID	Gene_name	Δβ
Hyper	103347582	leucine-rich repeat-containing protein 37A2-like(LOC103347582)	2,04
Hyper	100355489	cellular nucleic acid-binding protein(LOC100355489)	2,04
Hyper	100349806	39S ribosomal protein L53, mitochondrial pseudogene(LOC100349806)	2,09
Hyper	100352465	olfactory receptor 24(LOC100352465)	2,12
Hyper	100352569	fibroblast growth factor-binding protein 1-like(LOC100352569)	2,19
Hyper	103346476	leucine-rich repeat-containing protein 37A(LOC103346476)	2,21
Hyper	108176047	copine-8-like(LOC108176047)	2,24
Hyper	100352577	SUZ domain-containing protein 1 pseudogene(LOC100352577)	2,29
Hyper	100345416	coiled-coil-helix-coiled-coil-helix domain-containing protein 2 pseudogene(LOC100345416)	2,39
Hyper	103351282	peptidyl-prolyl cis-trans isomerase FKBP1A pseudogene(LOC103351282)	2,47
Hyper	100356042	hydroxyacyl-thioester dehydratase type 2, mitochondrial-like(LOC100356042)	2,58
Hyper	100345467	olfactory receptor 1361-like(LOC100345467)	2,60
Hyper	100356144	40S ribosomal protein S18(LOC100356144)	2,64
Hyper	100328969	octamer binding transcription factor 4 pseudogene(LOC100328969)	2,69
Hyper	108178276	H/ACA ribonucleoprotein complex subunit 3 pseudogene(LOC108178276)	2,70
Hyper	100349843	60S ribosomal protein L6 pseudogene(LOC100349843)	2,84
Hyper	100356483	ADP-ribosylation factor-like protein 5A pseudogene(LOC100356483)	2,85
Hyper	100348511	40S ribosomal protein S10(LOC100348511)	2,87
Hyper	100338371	olfactory receptor 2T11-like(LOC100338371)	3,07
Hyper	100349285	ferritin heavy chain pseudogene(LOC100349285)	3,16
Hyper	100346829	40S ribosomal protein S8 pseudogene(LOC100346829)	3,33
Hyper	100346219	deoxyuridine 5'-triphosphate nucleotidohydrolase, mitochondrial(LOC100346219)	3,36
Hyper	100355279	E3 ubiquitin-protein ligase RNF5-like(LOC100355279)	3,38
Hyper	100358370	60S ribosomal protein L15(LOC100358370)	3,40
Hyper	103345965	uncharacterized LOC103345965(LOC103345965)	3,41
Hyper	103346377	uncharacterized LOC103346377(LOC103346377)	4,21
Hyper	103351245	uncharacterized LOC103351245(LOC103351245)	4,24
Hyper	103346963	dihydropyrimidinase-related protein 2 pseudogene(LOC103346963)	4,43

Type	Gene_ID	Gene_name	Δβ
Hyper	103347197	leucine-rich repeat-containing protein 37A3 pseudogene(LOC103347197)	4,85
Hyper	100348047	UPF0561 protein C2orf68 homolog(LOC100348047)	4,92
Hyper	103346475	uncharacterized LOC103346475(LOC103346475)	5,05
Hyper	103347499	potassium voltage-gated channel subfamily D member 3 pseudogene(LOC103347499)	5,29
Hyper	108177361	uncharacterized LOC108177361(LOC108177361)	5,92
Hyper	103347602	uncharacterized LOC103347602(LOC103347602)	11,60
Hyper	108176300	leucine-rich repeat-containing protein 37A-like(LOC108176300)	13,34
Hyper	103347338	leucine-rich repeat-containing protein 37A3-like(LOC103347338)	30,67

Supplementary data 2. Functional analysis of differentially methylated genes of F0 in liver tissue due to effect of the embryo vitrification-transfer procedure.

Category	Type	Term	Count	P-Value
BP	Hypo	ATP synthesis coupled electron transport	2	0,02
BP	Hypo	UV protection	2	0,03
BP	Hypo	mitochondrial electron transport, NADH to ubiquinone	2	0,04
BP	Hypo	ATP synthesis coupled proton transport	2	0,08
BP	Hyper	translation	9	0,00
BP	Hyper	defense response to virus	2	0,09
CC	Hypo	mitochondrial respiratory chain complex I	5	0,00
CC	Hypo	respiratory chain	3	0,00
CC	Hypo	respiratory chain complex IV	2	0,02
CC	Hypo	mitochondrial proton-transporting ATP synthase complex	2	0,02
CC	Hypo	mitochondrion	9	0,03
CC	Hypo	integral component of membrane	27	0,06
CC	Hyper	ribosome	5	0,00
CC	Hyper	cytosolic small ribosomal subunit	3	0,00
CC	Hyper	membrane	5	0,02
CC	Hyper	nucleolus	4	0,03
CC	Hyper	cytosolic large ribosomal subunit	2	0,03
CC	Hyper	focal adhesion	3	0,06
MF	Hypo	NADH dehydrogenase (ubiquinone) activity	7	0,00
MF	Hypo	cytochrome-c oxidase activity	3	0,00
MF	Hypo	oxidoreductase activity	3	0,07
MF	Hypo	hydrogen ion transmembrane transporter activity	2	0,10
MF	Hyper	structural constituent of ribosome	9	0,00
MF	Hyper	cytochrome-c oxidase activity	2	0,03
MF	Hyper	poly(A) RNA binding	5	0,04
Kegg	Hypo	Parkinson's disease	13	0,00
Kegg	Hypo	Oxidative phosphorylation	12	0,00
Kegg	Hypo	Metabolic pathways	23	0,00
Kegg	Hypo	Alzheimer's disease	8	0,00
Kegg	Hypo	Huntington's disease	7	0,01

Category	Type	Term	Count	P-Value
Kegg	Hyper	Ribosome	6	0,00
Kegg	Hyper	Olfactory transduction	10	0,01
Kegg	Hyper	Pyruvate metabolism	3	0,02
Kegg	Hyper	RIG-I-like receptor signaling pathway	3	0,04

Supplementary data 3. Differentially methylated genes of F1 in liver tissue due to effect of the embryo vitrification-transfer procedure.

Type	Gene_ID	Gene_Name	Δβ
Hypo	108177834	transfer RNA leucine (anticodon CAG)(TRNAL-CAG)	-25,71
Hypo	108177775	transfer RNA glutamic acid (anticodon CUC)(TRNAE-CUC)	-24,30
Hypo	108177774	transfer RNA aspartic acid (anticodon GUC)(TRNAD-GUC)	-20,59
Hypo	100345911	high mobility group protein B2 pseudogene(LOC100345911)	-18,79
Hypo	103348463	TBC1 domain family member 26(LOC103348463)	-15,18
Hypo	108177772	transfer RNA glutamic acid (anticodon CUC)(TRNAE-CUC)	-11,20
Hypo	103348464	USP6 N-terminal-like protein(LOC103348464)	-9,67
Hypo	103347449	uncharacterized LOC103347449(LOC103347449)	-6,46
Hypo	103349199	IQ motif and SEC7 domain-containing protein 1-like(LOC103349199)	-5,98
Hypo	108178665	uncharacterized LOC108178665(LOC108178665)	-4,91
Hypo	108177100	uncharacterized LOC108177100(LOC108177100)	-4,62
Hypo	103346453	E3 ubiquitin-protein ligase UHRF2 pseudogene(LOC103346453)	-4,43
Hypo	108178781	uncharacterized LOC108178781(LOC108178781)	-3,83
Hypo	100352445	40S ribosomal protein S2 pseudogene(LOC100352445)	-3,72
Hypo	108176832	syncytin-2-like(LOC108176832)	-3,58
Hypo	100346763	UPF0235 protein C15orf40 homolog pseudogene(LOC100346763)	-3,39
Hypo	108175390	uncharacterized LOC108175390(LOC108175390)	-3,29
Hypo	108176217	U6 snRNA-associated Sm-like protein LSm3 pseudogene(LOC108176217)	-3,23
Hypo	108176831	endogenous retrovirus group K member 8 Pol protein-like(LOC108176831)	-3,23
Hypo	103346143	phosphatidylethanolamine binding protein 4(PEBP4)	-3,13
Hypo	100350561	multiple inositol polyphosphate phosphatase 1-like(LOC100350561)	-2,89
Hypo	100337813	cysteine-rich protein 2-like(LOC100337813)	-2,83
Hypo	103347487	putative ATP-dependent RNA helicase TDRD12(LOC103347487)	-2,78
Hypo	100354234	60S ribosomal protein L31 pseudogene(LOC100354234)	-2,54
Hypo	103347117	uncharacterized LOC103347117(LOC103347117)	-2,45
Hypo	100353758	SWI/SNF-related matrix-associated actin-dependent regulator of chromatin subfamily E member 1 pseudogene(LOC100353758)	-2,44
Hypo	108176951	cytochrome c oxidase subunit 6A1, mitochondrial pseudogene(LOC108176951)	-2,44
Hypo	100359278	sugar transporter SWEET1 pseudogene(LOC100359278)	-2,36
Hypo	108177909	syncytin-2-like(LOC108177909)	-2,34
Hypo	103348948	protein NipSnap homolog 2 pseudogene(LOC103348948)	-2,15
Hypo	100349429	zinc finger protein Pegasus pseudogene(LOC100349429)	-2,11
Hypo	100338584	ras-related protein Rap-1b pseudogene(LOC100338584)	-2,07
Hypo	108176334	transfer RNA leucine (anticodon CAG)(TRNAL-CAG)	-2,00
Hypo	100339133	40S ribosomal protein S6(LOC100339133)	-2,00
Hypo	100343630	exosome complex component CSL4 pseudogene(LOC100343630)	-1,99
Hypo	108177453	thymosin beta-10 pseudogene(LOC108177453)	-1,96
Hypo	808223	NADH dehydrogenase subunit 6(ND6)	-1,96
Hypo	100345096	p53 apoptosis effector related to PMP-22 pseudogene(LOC100345096)	-1,94

Type	Gene_ID	Gene_Name	Δβ
Hypo	100351483	H/ACA ribonucleoprotein complex subunit 2 pseudogene(LOC100351483)	-1,93
Hypo	108177184	60S ribosomal protein L23a(LOC108177184)	-1,91
Hypo	100345206	eukaryotic translation initiation factor 1A, X-chromosomal-like(LOC100345206)	-1,84
Hypo	108176236	carboxypeptidase E-like(LOC108176236)	-1,81
Hypo	100349729	putative 60S ribosomal protein L37a(LOC100349729)	-1,80
Hypo	808227	cytochrome b(CYTB)	-1,79
Hypo	108178912	40S ribosomal protein S11-like(LOC108178912)	-1,79
Hypo	100340730	claudin 22(CLDN22)	-1,78
Hypo	103347115	uncharacterized LOC103347115(LOC103347115)	-1,77
Hypo	100339296	uncharacterized LOC100339296(LOC100339296)	-1,75
Hypo	108177450	endogenous retrovirus group K member 11 Pol protein-like(LOC108177450)	-1,74
Hypo	108175851	ADP-ribosylation factor-like protein 6-interacting protein 6 pseudogene(LOC108175851)	-1,71
Hypo	808224	NADH dehydrogenase subunit 5(ND5)	-1,71
Hypo	108177245	endogenous retrovirus group K member 25 Pol protein-like(LOC108177245)	-1,71
Hypo	100356685	F-actin-capping protein subunit alpha-2-like(LOC100356685)	-1,67
Hypo	100344920	ATPase inhibitor, mitochondrial pseudogene(LOC100344920)	-1,66
Hypo	100358768	NF-kappa-B-activating protein pseudogene(LOC100358768)	-1,66
Hypo	108178565	endogenous retrovirus group K member 9 Pol protein-like(LOC108178565)	-1,65
Hypo	108176180	uncharacterized LOC108176180(LOC108176180)	-1,64
Hypo	100338456	m7GpppX diphosphatase(LOC100338456)	-1,63
Hypo	100346554	40S ribosomal protein SA pseudogene(LOC100346554)	-1,62
Hypo	103344974	40S ribosomal protein S4-like(LOC103344974)	-1,60
Hypo	108176634	60S ribosomal protein L17 pseudogene(LOC108176634)	-1,59
Hypo	103349197	uncharacterized LOC103349197(LOC103349197)	-1,55
Hypo	100344501	set1/Ash2 histone methyltransferase complex subunit ASH2 pseudogene(LOC100344501)	-1,55
Hypo	100009298	protein phosphatase 1 catalytic subunit alpha(PPP1CA)	-1,54
Hypo	103349139	uncharacterized LOC103349139(LOC103349139)	-1,53
Hypo	108176181	glia maturation factor beta pseudogene(LOC108176181)	-1,53
Hypo	108178494	transfer RNA asparagine (anticodon GUU)(TRNAN-GUU)	-1,53
Hypo	100343577	RNA-binding protein EWS pseudogene(LOC100343577)	-1,52
Hypo	100347165	60S ribosomal protein L34 pseudogene(LOC100347165)	-1,50
Hypo	100357921	bromodomain-containing protein 2 pseudogene(LOC100357921)	-1,50
Hypo	103345144	uncharacterized LOC103345144(LOC103345144)	-1,49
Hypo	108178368	26S proteasome complex subunit DSS1(LOC108178368)	-1,48
Hypo	100357158	complex I assembly factor TIMMDC1, mitochondrial pseudogene(LOC100357158)	-1,48
Hypo	108178560	nuclease-sensitive element-binding protein 1 pseudogene(LOC108178560)	-1,47
Hypo	100352196	nuclease-sensitive element-binding protein 1 pseudogene(LOC100352196)	-1,47
Hypo	100341852	cytochrome c-like(LOC100341852)	-1,47

Type	Gene_ID	Gene_Name	Δβ
Hypo	100347982	cyclin-dependent kinases regulatory subunit 2 pseudogene(LOC100347982)	-1,46
Hypo	103347079	histone-lysine N-methyltransferase SETD7(LOC103347079)	-1,45
Hypo	100354980	ribosomal protein L22(RPL22)	-1,45
Hypo	100347491	60S ribosomal protein L32 pseudogene(LOC100347491)	-1,44
Hypo	100341489	60S ribosomal protein L7 pseudogene(LOC100341489)	-1,43
Hypo	100358241	stathmin(LOC100358241)	-1,42
Hypo	108175773	ADP/ATP translocase 2-like(LOC108175773)	-1,42
Hypo	108178879	40S ribosomal protein S6(LOC108178879)	-1,42
Hypo	100345222	charged multivesicular body protein 3 pseudogene(LOC100345222)	-1,42
Hypo	108176175	uncharacterized LOC108176175(LOC108176175)	-1,41
Hypo	108177690	dolichyl-diphosphooligosaccharide--protein glycosyltransferase subunit 4(LOC108177690)	-1,40
Hypo	100353777	60S ribosomal protein L32 pseudogene(LOC100353777)	-1,40
Hypo	100358777	60S ribosomal protein L36a-like(LOC100358777)	-1,38
Hypo	100350662	membrane magnesium transporter 1 pseudogene(LOC100350662)	-1,38
Hypo	100349928	40S ribosomal protein S19 pseudogene(LOC100349928)	-1,37
Hypo	100338225	olfactory receptor 6C74-like(LOC100338225)	-1,36
Hypo	108178455	mitochondrial import receptor subunit TOM7 homolog pseudogene(LOC108178455)	-1,35
Hypo	100356206	histone H3.3-like(LOC100356206)	-1,35
Hypo	100348483	40S ribosomal protein S3a pseudogene(LOC100348483)	-1,33
Hypo	100338504	60S ribosomal protein L32 pseudogene(LOC100338504)	-1,33
Hypo	108176602	cytochrome c oxidase subunit 7C, mitochondrial pseudogene(LOC108176602)	-1,33
Hypo	100009168	serum amyloid protein A(LOC100009168)	-1,33
Hypo	100342995	28S ribosomal protein S21, mitochondrial pseudogene(LOC100342995)	-1,31
Hypo	100357927	histone H3.3-like(LOC100357927)	-1,30
Hypo	100346096	ATP synthase subunit f, mitochondrial(LOC100346096)	-1,30
Hypo	100345863	ubiquitin-conjugating enzyme E2 L3 pseudogene(LOC100345863)	-1,29
Hypo	100351486	40S ribosomal protein S10 pseudogene(LOC100351486)	-1,28
Hypo	100340418	nuclease-sensitive element-binding protein 1 pseudogene(LOC100340418)	-1,28
Hypo	100341684	ubiquitin-conjugating enzyme E2 N-like(LOC100341684)	-1,28
Hypo	100353293	poly(rC)-binding protein 2-like(LOC100353293)	-1,28
Hypo	100354151	retinal rod rhodopsin-sensitive cGMP 3',5'-cyclic phosphodiesterase subunit delta pseudogene(LOC100354151)	-1,27
Hypo	103345470	uncharacterized LOC103345470(LOC103345470)	-1,26
Hypo	100358283	40S ribosomal protein S11-like(LOC100358283)	-1,25
Hypo	100346519	60S ribosomal protein L32 pseudogene(LOC100346519)	-1,25
Hypo	100353361	60S ribosomal protein L37a-like(LOC100353361)	-1,25
Hypo	100339556	armadillo repeat-containing protein 1 pseudogene(LOC100339556)	-1,24
Hypo	100346642	60S ribosomal protein L32 pseudogene(LOC100346642)	-1,23
Hypo	100340971	60S ribosomal protein L38 pseudogene(LOC100340971)	-1,22
Hypo	100339500	zinc finger protein 791-like(LOC100339500)	-1,21
Hypo	100340708	40S ribosomal protein S3a pseudogene(LOC100340708)	-1,21

Type	Gene_ID	Gene_Name	Δβ
Hypo	100351957	60S ribosomal protein L6 pseudogene(LOC100351957)	-1,21
Hypo	108177743	60S ribosomal protein L36a-like(LOC108177743)	-1,19
Hypo	100356881	PCNA-associated factor-like(LOC100356881)	-1,19
Hypo	108175512	complex I assembly factor TMEM126B, mitochondrial pseudogene(LOC108175512)	-1,19
Hypo	100338583	DIS3-like exonuclease 1(LOC100338583)	-1,18
Hypo	103346813	E3 ubiquitin-protein ligase UHRF2 pseudogene(LOC103346813)	-1,17
Hypo	100358020	translationally-controlled tumor protein pseudogene(LOC100358020)	-1,17
Hypo	100341876	membrane cofactor protein-like(LOC100341876)	-1,16
Hypo	108175973	serine/arginine repetitive matrix protein 1 pseudogene(LOC108175973)	-1,16
Hypo	100358069	60S ribosomal protein L36a(LOC100358069)	-1,15
Hypo	100342151	kelch like family member 11(KLHL11)	-1,15
Hypo	100349264	RNA-binding protein 3 pseudogene(LOC100349264)	-1,15
Hypo	108177423	60S ribosomal protein L39(LOC108177423)	-1,14
Hypo	108178828	endogenous retrovirus group K member 8 Pol protein-like(LOC108178828)	-1,13
Hypo	100358185	L-lactate dehydrogenase B chain pseudogene(LOC100358185)	-1,12
Hypo	108177154	uncharacterized LOC108177154(LOC108177154)	-1,11
Hypo	108177809	transfer RNA glycine (anticodon CCC)(TRNAG-CCC)	-1,11
Hypo	100340865	polyadenylate-binding protein 1 pseudogene(LOC100340865)	-1,11
Hypo	103346495	tRNA-splicing ligase RtcB homolog pseudogene(LOC103346495)	-1,11
Hypo	100355704	ras-related protein Rab-22A pseudogene(LOC100355704)	-1,11
Hypo	808228	ATP synthase F0 subunit 8(ATP8)	-1,10
Hypo	100009281	RAB2A, member RAS oncogene family(RAB2A)	-1,10
Hypo	100345795	L-lactate dehydrogenase A chain pseudogene(LOC100345795)	-1,08
Hypo	100355297	60S ribosomal protein L17 pseudogene(LOC100355297)	-1,07
Hypo	100348970	10 kDa heat shock protein, mitochondrial pseudogene(LOC100348970)	-1,07
Hypo	100358630	peptidyl-prolyl cis-trans isomerase A pseudogene(LOC100358630)	-1,06
Hypo	100359068	ubiquitin-conjugating enzyme E2 L3 pseudogene(LOC100359068)	-1,06
Hypo	100341269	S-phase kinase-associated protein 1 pseudogene(LOC100341269)	-1,06
Hypo	108177053	small ubiquitin-related modifier 2 pseudogene(LOC108177053)	-1,05
Hypo	100349893	tropomyosin alpha-3 chain(LOC100349893)	-1,03
Hypo	100338960	40S ribosomal protein S6 pseudogene(LOC100338960)	-1,03
Hypo	100356310	40S ribosomal protein S26-like(LOC100356310)	-1,03
Hypo	100339297	60S ribosomal protein L12 pseudogene(LOC100339297)	-1,02
Hypo	100350326	dihydrofolate reductase-like(LOC100350326)	-1,02
Hypo	808230	NADH dehydrogenase subunit 2(ND2)	-1,02
Hypo	100343039	60S ribosomal protein L21(LOC100343039)	-1,01
Hypo	108175579	transfer RNA valine (anticodon AAC)(TRNAV-AAC)	-1,01
Hypo	103349296	nucleosome assembly protein 1-like 1 pseudogene(LOC103349296)	-1,01
Hypo	108175857	40S ribosomal protein S6 pseudogene(LOC108175857)	-1,01
Hypo	808233	cytochrome c oxidase subunit II(COX2)	-1,00
Hypo	100353447	26S proteasome non-ATPase regulatory subunit 10 pseudogene(LOC100353447)	-1,00

Type	Gene_ID	Gene_Name	Δβ
Hypo	100351336	60S ribosomal protein L9 pseudogene(LOC100351336)	-0,99
Hypo	100339073	protein SDA1 homolog(LOC100339073)	-0,99
Hypo	103351723	Ig lambda chain V-VI region WLT-like(LOC103351723)	-0,99
Hypo	100341783	60S ribosomal protein L23(LOC100341783)	-0,98
Hypo	100343583	HIG1 domain family member 1A, mitochondrial pseudogene(LOC100343583)	-0,98
Hypo	808221	NADH dehydrogenase subunit 3(ND3)	-0,98
Hypo	108177372	endogenous retrovirus group K member 9 Pol protein-like(LOC108177372)	-0,98
Hypo	100357329	cytochrome c(LOC100357329)	-0,98
Hypo	100349832	mitochondrial import inner membrane translocase subunit Tim8 A pseudogene(LOC100349832)	-0,98
Hypo	108176769	transfer RNA glycine (anticodon GCC)(TRNAG-GCC)	-0,97
Hypo	108176357	gamma-aminobutyric acid receptor-associated protein-like 2 pseudogene(LOC108176357)	-0,97
Hypo	100342981	small ubiquitin-related modifier 2 pseudogene(LOC100342981)	-0,96
Hypo	100344452	small ubiquitin-related modifier 2 pseudogene(LOC100344452)	-0,96
Hypo	100356896	60S ribosomal protein L22-like 1 pseudogene(LOC100356896)	-0,95
Hypo	100355943	plasminogen activator inhibitor 1 RNA-binding protein pseudogene(LOC100355943)	-0,95
Hypo	100342136	UPF0568 protein C14orf166 pseudogene(LOC100342136)	-0,95
Hypo	808229	cytochrome c oxidase subunit III(COX3)	-0,93
Hypo	100356718	partner of NOB1 homolog(PNO1)	-0,93
Hypo	108175530	transfer RNA leucine (anticodon CAA)(TRNAL-CAA)	-0,93
Hypo	103346406	biogenesis of lysosome-related organelles complex 1 subunit 5 pseudogene(LOC103346406)	-0,92
Hypo	108175625	protein phosphatase 1 regulatory subunit 3D(PPP1R3D)	-0,92
Hypo	100340132	small ubiquitin-related modifier 2(LOC100340132)	-0,92
Hypo	100357648	chromosome 10 open reading frame, human C7orf62(C10H7orf62)	-0,91
Hypo	100353915	60S ribosomal protein L17 pseudogene(LOC100353915)	-0,90
Hypo	100358879	transcription initiation factor TFIID subunit 9-like(LOC100358879)	-0,90
Hypo	108177658	small nuclear ribonucleoprotein G pseudogene(LOC108177658)	-0,88
Hypo	108176564	endogenous retrovirus group K member 9 Pol protein-like(LOC108176564)	-0,88
Hypo	103344953	protein SET-like(LOC103344953)	-0,88
Hypo	100355447	heterogeneous nuclear ribonucleoprotein H2-like(LOC100355447)	-0,87
Hypo	100342527	60S ribosomal protein L26 pseudogene(LOC100342527)	-0,87
Hypo	100338711	40S ribosomal protein S3a pseudogene(LOC100338711)	-0,87
Hypo	100353295	60S ribosomal protein L35a pseudogene(LOC100353295)	-0,87
Hypo	808225	NADH dehydrogenase subunit 4(ND4)	-0,87
Hypo	100356908	SS18-like protein 2 pseudogene(LOC100356908)	-0,86
Hypo	103350176	zinc finger protein 684-like(LOC103350176)	-0,86
Hypo	100351933	NADH dehydrogenase [ubiquinone] 1 beta subcomplex subunit 4 pseudogene(LOC100351933)	-0,86
Hypo	100341105	membrane cofactor protein-like(LOC100341105)	-0,85
Hypo	100341154	single-stranded DNA-binding protein, mitochondrial pseudogene(LOC100341154)	-0,85
Hypo	103348454	uncharacterized LOC103348454(LOC103348454)	-0,85

Type	Gene_ID	Gene_Name	Δβ
Hypo	100354914	putative olfactory receptor 10D4(LOC100354914)	-0,85
Hypo	100345152	protein-lysine methyltransferase METTL21D pseudogene(LOC100345152)	-0,84
Hypo	108175790	endogenous retrovirus group K member 7 Pro protein-like(LOC108175790)	-0,84
Hypo	103348330	uncharacterized LOC103348330(LOC103348330)	-0,83
Hypo	100349685	small nuclear ribonucleoprotein Sm D1 pseudogene(LOC100349685)	-0,83
Hypo	808231	cytochrome c oxidase subunit I(COX1)	-0,82
Hypo	100346801	PRELI domain containing protein 3B pseudogene(LOC100346801)	-0,82
Hypo	100344215	ubiquitin-fold modifier 1 pseudogene(LOC100344215)	-0,82
Hypo	808232	ATP synthase F0 subunit 6(ATP6)	-0,81
Hypo	103347575	uncharacterized LOC103347575(LOC103347575)	-0,81
Hypo	100341292	putative 60S ribosomal protein L37a(LOC100341292)	-0,80
Hypo	108178002	60S ribosomal protein L31 pseudogene(LOC108178002)	-0,80
Hypo	100357142	40S ribosomal protein S12 pseudogene(LOC100357142)	-0,80
Hypo	103349409	pre-mRNA-splicing factor ATP-dependent RNA helicase DHX15 pseudogene(LOC103349409)	-0,77
Hypo	100354760	60S ribosomal protein L9(LOC100354760)	-0,76
Hypo	100340097	ankyrin repeat family A member 2(ANKRA2)	-0,76
Hypo	108177297	ubiquitin-conjugating enzyme E2 variant 2 pseudogene(LOC108177297)	-0,76
Hypo	103346924	uncharacterized LOC103346924(LOC103346924)	-0,76
Hypo	100347116	cyclin-C pseudogene(LOC100347116)	-0,75
Hypo	108176592	transfer RNA tyrosine (anticodon GUA)(TRNAY-GUA)	-0,74
Hypo	103347765	Ig kappa chain V region 3381-like(LOC103347765)	-0,74
Hypo	100340201	SOSS complex subunit C pseudogene(LOC100340201)	-0,73
Hypo	100350993	uncharacterized protein C14orf142 pseudogene(LOC100350993)	-0,73
Hypo	100356235	60S ribosomal protein L26-like(LOC100356235)	-0,72
Hypo	108177303	transfer RNA aspartic acid (anticodon GUC)(TRNAD-GUC)	-0,72
Hypo	100355466	non-histone chromosomal protein HMG-14 pseudogene(LOC100355466)	-0,72
Hypo	808222	NADH dehydrogenase subunit 4L(ND4L)	-0,72
Hypo	100351260	small nuclear ribonucleoprotein E pseudogene(LOC100351260)	-0,71
Hypo	100349585	ADP-ribosylation factor-like protein 1 pseudogene(LOC100349585)	-0,70
Hypo	100357123	translationally-controlled tumor protein pseudogene(LOC100357123)	-0,70
Hypo	100347060	protein SSXT-like(LOC100347060)	-0,70
Hypo	100354530	destrin pseudogene(LOC100354530)	-0,70
Hypo	100357151	protein disulfide-isomerase A3-like(LOC100357151)	-0,70
Hypo	100344405	40S ribosomal protein S27-like(LOC100344405)	-0,69
Hypo	100344250	ubiquitin-conjugating enzyme E2 variant 2 pseudogene(LOC100344250)	-0,69
Hypo	808226	NADH dehydrogenase subunit 1(ND1)	-0,68
Hypo	108177503	transfer RNA isoleucine (anticodon UAU)(TRNAI-UAU)	-0,68
Hypo	100341169	oligosaccharyltransferase complex subunit OSTC pseudogene(LOC100341169)	-0,68
Hypo	108178135	transfer RNA methionine (anticodon CAU)(TRNAM-CAU)	-0,67
Hypo	100339717	ubiquitin-conjugating enzyme E2 D3 pseudogene(LOC100339717)	-0,66

Type	Gene_ID	Gene_Name	Δβ
Hypo	100354062	heterogeneous nuclear ribonucleoprotein C pseudogene(LOC100354062)	-0,66
Hypo	103348093	uncharacterized LOC103348093(LOC103348093)	-0,66
Hypo	100357434	polyadenylate-binding protein-interacting protein 1 pseudogene(LOC100357434)	-0,64
Hypo	108178282	40S ribosomal protein SA-like(LOC108178282)	-0,64
Hypo	103349294	ankyrin repeat domain-containing protein 12-like(LOC103349294)	-0,64
Hypo	100351304	succinate dehydrogenase [ubiquinone] cytochrome b small subunit, mitochondrial pseudogene(LOC100351304)	-0,63
Hypo	100356093	vinculin-like(LOC100356093)	-0,63
Hypo	100350038	ribosome biogenesis protein NSA2 homolog pseudogene(LOC100350038)	-0,63
Hypo	100353434	ret finger protein-like 4B(LOC100353434)	-0,63
Hypo	100357742	PEST proteolytic signal-containing nuclear protein(LOC100357742)	-0,61
Hypo	100346768	meiotic nuclear division protein 1 homolog(LOC100346768)	-0,60
Hypo	100344395	rRNA-processing protein FCF1 homolog pseudogene(LOC100344395)	-0,60
Hypo	100344743	40S ribosomal protein S6 pseudogene(LOC100344743)	-0,60
Hypo	100349973	protein LSM12 homolog pseudogene(LOC100349973)	-0,60
Hypo	100355699	60S ribosomal protein L27 pseudogene(LOC100355699)	-0,60
Hypo	100348679	RRP15-like protein pseudogene(LOC100348679)	-0,57
Hypo	100339978	DNA primase small subunit pseudogene(LOC100339978)	-0,57
Hypo	108176577	focal adhesion kinase 1 pseudogene(LOC108176577)	-0,56
Hypo	100359038	pleckstrin homology domain containing B2(PLEKHB2)	-0,56
Hypo	100345528	transcription elongation factor B polypeptide 1 pseudogene(LOC100345528)	-0,56
Hypo	108177855	transfer RNA arginine (anticodon UCU)(TRNAR-UCU)	-0,55
Hypo	100345559	putative gustatory receptor clone PTE01(LOC100345559)	-0,53
Hypo	100340862	ras-related protein Rap-1b-like protein(LOC100340862)	-0,53
Hypo	100343112	putative 60S ribosomal protein L37a(LOC100343112)	-0,53
Hypo	103350788	ADP-ribosylation factor-like protein 1 pseudogene(LOC103350788)	-0,52
Hypo	100341000	OTU domain-containing protein 4-like(LOC100341000)	-0,52
Hypo	100358709	phospholipase A2 group XIIA(PLA2G12A)	-0,50
Hypo	108176275	glutamate receptor ionotropic, NMDA 2A pseudogene(LOC108176275)	-0,50
Hypo	100355052	trace amine-associated receptor 8-like(LOC100355052)	-0,49
Hypo	100343801	adenosine deaminase-like protein pseudogene(LOC100343801)	-0,49
Hypo	108178858	dolichyl-diphosphooligosaccharide--protein glycosyltransferase subunit 4-like(LOC108178858)	-0,48
Hypo	100349495	28S ribosomal protein S17, mitochondrial(LOC100349495)	-0,46
Hypo	108176378	uncharacterized LOC108176378(LOC108176378)	-0,45
Hypo	103351489	transcription factor BTF3 homolog 4 pseudogene(LOC103351489)	-0,42
Hypo	100347591	BAG family molecular chaperone regulator 2 pseudogene(LOC100347591)	-0,40
Hypo	100339231	protein MEMO1 pseudogene(LOC100339231)	-0,39
Hypo	104795870	microRNA 302b(MIR302B)	-0,38
Hypo	100341160	lysozyme C(LOC100341160)	-0,38
Hypo	108178609	transfer RNA cysteine (anticodon GCA)(TRNAC-GCA)	-0,37
Hyper	100354286	T-complex protein 1 subunit zeta pseudogene(LOC100354286)	0,36

Type	Gene_ID	Gene_Name	Δβ
Hyper	108177852	transfer RNA asparagine (anticodon GUU)(TRNAN-GUU)	0,40
Hyper	103346787	chromosome unknown open reading frame, human C19orf70(LOC103346787)	0,44
Hyper	108175635	T-cell receptor beta chain V region CTL-L17-like(LOC108175635)	0,50
Hyper	100349054	kinetochore protein Spc25 pseudogene(LOC100349054)	0,51
Hyper	108178389	transfer RNA threonine (anticodon UGU)(TRNAT-UGU)	0,53
Hyper	100356497	poly(rC)-binding protein 2-like(LOC100356497)	0,55
Hyper	100353830	cyclin-C pseudogene(LOC100353830)	0,58
Hyper	108178980	S100P-binding protein-like(LOC108178980)	0,59
Hyper	108176298	uncharacterized LOC108176298(LOC108176298)	0,59
Hyper	108178377	transfer RNA threonine (anticodon UGU)(TRNAT-UGU)	0,60
Hyper	100347177	60S ribosomal protein L27 pseudogene(LOC100347177)	0,61
Hyper	100348667	heterogeneous nuclear ribonucleoprotein A3-like(LOC100348667)	0,62
Hyper	108175722	killer cell lectin-like receptor 8(LOC108175722)	0,65
Hyper	108178254	uncharacterized LOC108178254(LOC108178254)	0,67
Hyper	100009424	adrenoceptor alpha 2A(ADRA2A)	0,68
Hyper	100348088	prefoldin subunit 6 pseudogene(LOC100348088)	0,69
Hyper	100342813	regulatory subunit of type II PKA R-subunit (RIIa) domain containing 1(RIIAD1)	0,70
Hyper	100356572	heat shock cognate 71 kDa protein pseudogene(LOC100356572)	0,76
Hyper	100352010	prefoldin subunit 6(PFDN6)	0,77
Hyper	108175982	uncharacterized LOC108175982(LOC108175982)	0,78
Hyper	103345565	goosecoid homeobox 2(GSC2)	0,78
Hyper	103346928	uncharacterized LOC103346928(LOC103346928)	0,78
Hyper	100345620	homeobox B13(HOXB13)	0,79
Hyper	100344139	glucosamine 6-phosphate N-acetyltransferase pseudogene(LOC100344139)	0,80
Hyper	108178018	60S ribosomal protein L17 pseudogene(LOC108178018)	0,81
Hyper	108178868	butyrophilin subfamily 2 member A2-like(LOC108178868)	0,82
Hyper	100337740	trichohyalin(TCHH)	0,83
Hyper	103346408	uncharacterized LOC103346408(LOC103346408)	0,84
Hyper	108175634	T-cell receptor beta chain V region PHDS203-like(LOC108175634)	0,84
Hyper	103347844	uncharacterized LOC103347844(LOC103347844)	0,84
Hyper	100338841	keratin-associated protein 4-9-like(LOC100338841)	0,87
Hyper	100347461	adrenomedullin(ADM)	0,87
Hyper	100339330	E3 ubiquitin-protein ligase RNF138-like(LOC100339330)	0,89
Hyper	103347754	Ig kappa chain V region 3381-like(LOC103347754)	0,89
Hyper	108178819	zinc finger protein 367-like(LOC108178819)	0,89
Hyper	100358452	transcription elongation factor A protein 1-like(LOC100358452)	0,90
Hyper	103347513	stabilin-2(LOC103347513)	0,92
Hyper	108176246	transfer RNA asparagine (anticodon GUU)(TRNAN-GUU)	0,92
Hyper	100345190	ubiquitin-conjugating enzyme E2 L3(LOC100345190)	0,94
Hyper	100348318	survival motor neuron protein-like(LOC100348318)	0,96
Hyper	100350315	prostaglandin E synthase 3 pseudogene(LOC100350315)	0,96
Hyper	108176728	uncharacterized LOC108176728(LOC108176728)	0,97

Type	Gene_ID	Gene_Name	Δβ
Hyper	100342943	fibroblast growth factor 4(FGF4)	0,97
Hyper	100355237	HscB mitochondrial iron-sulfur cluster cochaperone(HSCB)	0,98
Hyper	100341251	ribosomal protein L26 like 1(RPL26L1)	0,98
Hyper	108176089	regulator of G-protein signaling 2-like(LOC108176089)	0,99
Hyper	103348484	uncharacterized LOC103348484(LOC103348484)	0,99
Hyper	108175412	OTU deubiquitinase 1(OTUD1)	0,99
Hyper	103348616	uncharacterized LOC103348616(LOC103348616)	1,00
Hyper	103351128	uncharacterized LOC103351128(LOC103351128)	1,00
Hyper	108175472	trafficking protein particle complex subunit 9-like(LOC108175472)	1,01
Hyper	100344617	60S ribosomal protein L15 pseudogene(LOC100344617)	1,01
Hyper	103347536	1-phosphatidylinositol 4,5-bisphosphate phosphodiesterase beta-3-like(LOC103347536)	1,01
Hyper	100351709	olfactory receptor 7G2-like(LOC100351709)	1,02
Hyper	100349135	transmembrane protein 173(TMEM173)	1,02
Hyper	100355268	60S ribosomal protein L32 pseudogene(LOC100355268)	1,02
Hyper	103346177	scavenger receptor class F member 2(SCARF2)	1,02
Hyper	108178276	H/ACA ribonucleoprotein complex subunit 3 pseudogene(LOC108178276)	1,04
Hyper	108176356	60S ribosomal protein L36 pseudogene(LOC108176356)	1,05
Hyper	100342497	NKG2D ligand 1(LOC100342497)	1,06
Hyper	100343207	zinc finger CCHC-type and RNA-binding motif-containing protein 1 pseudogene(LOC100343207)	1,06
Hyper	100349810	olfactory receptor 2G6(LOC100349810)	1,07
Hyper	100342526	60S ribosomal protein L7 pseudogene(LOC100342526)	1,09
Hyper	103350704	small ubiquitin-related modifier 2 pseudogene(LOC103350704)	1,09
Hyper	100357625	beta-enolase pseudogene(LOC100357625)	1,10
Hyper	108176971	transfer RNA lysine (anticodon CUU)(TRNAK-CUU)	1,10
Hyper	103347295	NKG2D ligand 1(LOC103347295)	1,11
Hyper	100344199	maspardin-like(LOC100344199)	1,12
Hyper	108176303	NKG2D ligand 2-like(LOC108176303)	1,12
Hyper	103349508	glucosamine 6-phosphate N-acetyltransferase pseudogene(LOC103349508)	1,13
Hyper	100353228	prostaglandin E synthase 2(PTGES2)	1,13
Hyper	100350798	zymogen granule membrane protein 16(LOC100350798)	1,14
Hyper	100351806	uncharacterized LOC100351806(LOC100351806)	1,14
Hyper	103351079	mitochondrial import inner membrane translocase subunit TIM14 pseudogene(LOC103351079)	1,15
Hyper	100328583	GRO beta protein(GRO-B)	1,16
Hyper	108176260	NKG2D ligand 2-like(LOC108176260)	1,17
Hyper	108176792	uncharacterized LOC108176792(LOC108176792)	1,18
Hyper	108178977	collagen alpha-2(I) chain-like(LOC108178977)	1,18
Hyper	103347582	leucine-rich repeat-containing protein 37A2-like(LOC103347582)	1,19
Hyper	100351576	uncharacterized protein C6orf62 homolog pseudogene(LOC100351576)	1,20
Hyper	100347468	40S ribosomal protein S11(LOC100347468)	1,23
Hyper	100342515	ADP-ribosylation factor-like protein 5A pseudogene(LOC100342515)	1,26
Hyper	103346407	uncharacterized LOC103346407(LOC103346407)	1,28

Type	Gene_ID	Gene_Name	Δβ
Hyper	108176296	uncharacterized LOC108176296(LOC108176296)	1,31
Hyper	100351947	RAN guanine nucleotide release factor(RANGRF)	1,31
Hyper	100337833	keratin-associated protein 2-1-like(LOC100337833)	1,32
Hyper	103348167	uncharacterized LOC103348167(LOC103348167)	1,32
Hyper	100341682	syncollin(SYCN)	1,33
Hyper	100338084	adrenoceptor beta 1(ADRB1)	1,35
Hyper	108175654	T-cell receptor beta chain V region C5-like(LOC108175654)	1,37
Hyper	100340447	serine/arginine-rich splicing factor 11 pseudogene(LOC100340447)	1,37
Hyper	103351007	ADP ribosylation factor like GTPase 8A(ARL8A)	1,38
Hyper	100343444	heterogeneous nuclear ribonucleoprotein A1-like(LOC100343444)	1,40
Hyper	108177202	uncharacterized LOC108177202(LOC108177202)	1,41
Hyper	103347588	ral-GDS-related protein-like(LOC103347588)	1,42
Hyper	100344550	protein mago nashi homolog(LOC100344550)	1,43
Hyper	100345416	coiled-coil-helix-coiled-coil-helix domain-containing protein 2 pseudogene(LOC100345416)	1,43
Hyper	103347910	chromosome 3 open reading frame, human C5orf46(C3H5orf46)	1,46
Hyper	103346161	ral-GDS-related protein-like(LOC103346161)	1,52
Hyper	100328948	cytochrome P-450(LOC100328948)	1,52
Hyper	100355489	cellular nucleic acid-binding protein(LOC100355489)	1,56
Hyper	108178512	uncharacterized LOC108178512(LOC108178512)	1,56
Hyper	108176757	liver carboxylesterase 2-like(LOC108176757)	1,57
Hyper	100338481	non-histone chromosomal protein HMG-14(LOC100338481)	1,57
Hyper	103346280	insulin growth factor-like family member 4(LOC103346280)	1,60
Hyper	100343031	proteasome assembly chaperone 3(PSMG3)	1,61
Hyper	100339326	chymotrypsin-like elastase family member 3B(LOC100339326)	1,62
Hyper	100355793	shisa family member 5(SHISA5)	1,63
Hyper	100348402	KH domain containing 3 like, subcortical maternal complex member(KHDC3L)	1,63
Hyper	100008655	annexin A8(ANXA8)	1,65
Hyper	100343857	ribonuclease P/MRP subunit p25(RPP25)	1,66
Hyper	103346470	cyclin-dependent kinase 11B-like(LOC103346470)	1,69
Hyper	103347593	interferon-induced transmembrane protein 1-like(LOC103347593)	1,73
Hyper	103351133	uncharacterized LOC103351133(LOC103351133)	1,74
Hyper	100356483	ADP-ribosylation factor-like protein 5A pseudogene(LOC100356483)	1,80
Hyper	103346916	uncharacterized LOC103346916(LOC103346916)	1,81
Hyper	100349133	thymosin beta 10(TMSB10)	1,82
Hyper	108177869	transfer RNA asparagine (anticodon GUU)(TRNAN-GUU)	1,85
Hyper	100344166	phospholipase A2, membrane associated-like(LOC100344166)	1,85
Hyper	100349394	transducin-like enhancer protein 4 pseudogene(LOC100349394)	1,88
Hyper	100358934	Ig alpha chain C region-like(LOC100358934)	1,92
Hyper	103347044	uncharacterized LOC103347044(LOC103347044)	1,95
Hyper	100347275	uncharacterized LOC100347275(LOC100347275)	2,00
Hyper	103349137	IQ motif and SEC7 domain-containing protein 1-like(LOC103349137)	2,01
Hyper	108177974	60S ribosomal protein L23a(LOC108177974)	2,03
Hyper	100352577	SUZ domain-containing protein 1 pseudogene(LOC100352577)	2,07

Type	Gene_ID	Gene_Name	Δβ
Hyper	103346586	ral-GDS-related protein(LOC103346586)	2,15
Hyper	103347343	ral-GDS-related protein-like(LOC103347343)	2,15
Hyper	100347019	histone H2A type 1-H(LOC100347019)	2,18
Hyper	100338718	natriuretic peptides B-like(LOC100338718)	2,23
Hyper	100343565	integrin beta-1-binding protein 1 pseudogene(LOC100343565)	2,27
Hyper	103351169	T-cell receptor alpha chain V region PHDS58-like(LOC103351169)	2,28
Hyper	100348913	chymotrypsin-like elastase family member 3B(LOC100348913)	2,30
Hyper	108177590	forkhead box E3(FOXE3)	2,31
Hyper	100349843	60S ribosomal protein L6 pseudogene(LOC100349843)	2,33
Hyper	103346278	insulin growth factor-like family member 1(LOC103346278)	2,34
Hyper	100349634	synaptogyrin 4(SYNGR4)	2,35
Hyper	100341745	ras related dexamethasone induced 1(RASD1)	2,37
Hyper	100342121	40S ribosomal protein S14 pseudogene(LOC100342121)	2,43
Hyper	100339828	hyaluronan and proteoglycan link protein 2(HAPLN2)	2,46
Hyper	100356144	40S ribosomal protein S18(LOC100356144)	2,49
Hyper	100338371	olfactory receptor 2T11-like(LOC100338371)	2,56
Hyper	103347078	phosphatidylinositol 4-phosphate 5-kinase type-1 gamma pseudogene(LOC103347078)	2,57
Hyper	108176244	transfer RNA histidin (anticodon GUG)(TRNAH-GUG)	2,59
Hyper	100346829	40S ribosomal protein S8 pseudogene(LOC100346829)	2,62
Hyper	100345533	pre-B lymphocyte 1(VPREB1)	2,64
Hyper	100338136	nucleolar protein 3(NOL3)	2,67
Hyper	100338961	nuclear transcription factor Y subunit beta-like(LOC100338961)	2,69
Hyper	100357474	liver carboxylesterase 2-like(LOC100357474)	2,75
Hyper	100359144	ATP synthase F(0) complex subunit B1, mitochondrial-like(LOC100359144)	2,81
Hyper	108176099	uncharacterized LOC108176099(LOC108176099)	2,86
Hyper	103349667	brain acid soluble protein 1(LOC103349667)	2,88
Hyper	100357730	liver carboxylesterase 2-like(LOC100357730)	2,88
Hyper	100347640	60S ribosomal protein L15 pseudogene(LOC100347640)	2,89
Hyper	100350206	A-kinase anchor protein 8 pseudogene(LOC100350206)	3,04
Hyper	100338462	mitochondrial ribosomal protein L11(MRPL11)	3,10
Hyper	103347540	stathmin-3(LOC103347540)	3,19
Hyper	103346712	GPI transamidase component PIG-T pseudogene(LOC103346712)	3,22
Hyper	100008923	sterile alpha motif domain containing 1(SAMD1)	3,25
Hyper	100349285	ferritin heavy chain pseudogene(LOC100349285)	3,28
Hyper	100340623	mitochondrial import inner membrane translocase subunit Tim13 pseudogene(LOC100340623)	3,31
Hyper	100351367	DiGeorge syndrome critical region gene 6-like(DGCR6L)	3,39
Hyper	103347638	uncharacterized LOC103347638(LOC103347638)	3,42
Hyper	103347499	potassium voltage-gated channel subfamily D member 3 pseudogene(LOC103347499)	3,48
Hyper	100346271	zymogen granule membrane protein 16(LOC100346271)	3,52
Hyper	108176006	uncharacterized LOC108176006(LOC108176006)	3,68
Hyper	100316858	cytochrome P450 2D/II(CYP2D24)	3,73
Hyper	103346475	uncharacterized LOC103346475(LOC103346475)	3,96

Type	Gene_ID	Gene_Name	Δβ
Hyper	103346963	dihydropyrimidinase-related protein 2 pseudogene(LOC103346963)	4,09
Hyper	100340362	core-binding factor subunit beta-like(LOC100340362)	4,16
Hyper	103346387	spore coat protein SP85(LOC103346387)	4,24
Hyper	100355279	E3 ubiquitin-protein ligase RNF5-like(LOC100355279)	4,34
Hyper	103346648	protein C9orf69-like(LOC103346648)	4,34
Hyper	108176732	uncharacterized LOC108176732(LOC108176732)	4,46
Hyper	100339366	olfactory receptor 2T6-like(LOC100339366)	4,68
Hyper	103346480	translation initiation factor IF-2-like(LOC103346480)	4,80
Hyper	100358487	calcium release-activated calcium channel protein 1 pseudogene(LOC100358487)	4,81
Hyper	100356480	achaete-scute family bHLH transcription factor 5(ASCL5)	4,82
Hyper	103346164	protein RoBo-1(LOC103346164)	4,95
Hyper	104795877	microRNA 191(MIR191)	5,32
Hyper	100339911	succinyl-CoA:3-ketoacid coenzyme A transferase 2, mitochondrial-like(LOC100339911)	5,42
Hyper	100341662	neuronal acetylcholine receptor subunit alpha-10-like(LOC100341662)	5,43
Hyper	100342420	paired related homeobox 2(PRRX2)	5,56
Hyper	100354392	coiled-coil domain containing 8(CCDC8)	5,73
Hyper	108176147	extensin-like(LOC108176147)	5,86
Hyper	100343699	forkhead box protein R1 pseudogene(LOC100343699)	6,13
Hyper	108178915	uncharacterized LOC108178915(LOC108178915)	6,31
Hyper	100338613	serine/threonine-protein kinase LMTK3-like(LOC100338613)	6,42
Hyper	103344962	kelch-like protein 26(LOC103344962)	7,32
Hyper	100341474	cytochrome c oxidase subunit 6A2, mitochondrial(LOC100341474)	7,56
Hyper	108175433	histo-blood group ABO system transferase 2-like(LOC108175433)	8,42
Hyper	100357119	Krueppel-like factor 5 pseudogene(LOC100357119)	8,56
Hyper	103347352	histo-blood group ABO system transferase 2-like(LOC103347352)	8,69
Hyper	100357202	coiled-coil domain-containing protein 85C-like(LOC100357202)	10,30
Hyper	108175430	ATP synthase mitochondrial F1 complex assembly factor 2-like(LOC108175430)	11,99
Hyper	108176091	beta-galactosidase-like(LOC108176091)	13,58
Hyper	100328955	pre-B lymphocyte 2(VPREB2)	13,82
Hyper	103347179	transcription elongation factor SPT5(LOC103347179)	14,67
Hyper	100358140	endothelial differentiation-related factor 1 pseudogene(LOC100358140)	15,23
Hyper	103347196	uncharacterized LOC103347196(LOC103347196)	16,01
Hyper	103346389	phosphatidylinositol 4-phosphate 5-kinase type-1 gamma pseudogene(LOC103346389)	17,31
Hyper	100357882	Y-box-binding protein 2 pseudogene(LOC100357882)	19,58
Hyper	103346910	glucose-induced degradation protein 4 homolog(LOC103346910)	19,70
Hyper	108176090	homeobox protein SIX5-like(LOC108176090)	28,12
Hyper	100353654	basic proline-rich protein-like(LOC100353654)	45,61
Hyper	108176166	uncharacterized LOC108176166(LOC108176166)	99,90
Hyper	100328976	18S ribosomal RNA(RN18S)	248,33
Hyper	108176098	translation initiation factor IF-2-like(LOC108176098)	313,46

Supplementary data 4. Functional analysis of differentially methylated genes of F1 in liver tissue due to effect of the embryo vitrification-transfer procedure.

Category	Type	Term	Count	P-Value
BP	Hypo	translation	11	0,00
BP	Hypo	ATP synthesis coupled electron transport	2	0,01
BP	Hypo	ribosomal small subunit biogenesis	2	0,02
BP	Hypo	mitochondrial electron transport, NADH to ubiquinone	2	0,03
BP	Hypo	ATP synthesis coupled proton transport	2	0,05
BP	Hypo	TOR signaling	2	0,05
BP	Hypo	rRNA processing	2	0,09
BP	Hyper	translation	5	0,00
BP	Hyper	positive regulation of cAMP biosynthetic process	2	0,07
BP	Hyper	protein oligomerization	2	0,08
CC	Hypo	mitochondrial respiratory chain complex I	5	0,00
CC	Hypo	ribosome	6	0,00
CC	Hypo	respiratory chain complex IV	3	0,00
CC	Hypo	respiratory chain	3	0,00
CC	Hypo	cytosolic large ribosomal subunit	3	0,00
CC	Hypo	mitochondrial proton-transporting ATP synthase complex	2	0,01
CC	Hypo	integral component of membrane	18	0,03
CC	Hypo	cytoplasmic ribonucleoprotein granule	2	0,06
CC	Hypo	mitochondrial inner membrane	3	0,06
CC	Hypo	mitochondrial membrane	2	0,07
CC	Hypo	cell body	2	0,10
CC	Hypo	cytosolic small ribosomal subunit	2	0,10
CC	Hyper	extracellular region	4	0,06
CC	Hyper	cytosolic small ribosomal subunit	2	0,09
MF	Hypo	NADH dehydrogenase (ubiquinone) activity	7	0,00
MF	Hypo	structural constituent of ribosome	11	0,00
MF	Hypo	cytochrome-c oxidase activity	3	0,00
MF	Hypo	hydrogen ion transmembrane transporter activity	2	0,07
MF	Hyper	structural constituent of ribosome	5	0,00
MF	Hyper	oxidoreductase activity, acting on paired donors, with incorporation or reduction of molecular oxygen, reduced flavin or flavoprotein as one donor, and incorporation of one atom of oxygen	2	0,05
Kegg	Hypo	Oxidative phosphorylation	15	0,00
Kegg	Hypo	Parkinson's disease	15	0,00
Kegg	Hypo	Ribosome	12	0,00

Category	Type	Term	Count	P-Value
Kegg	Hypo	Alzheimer's disease	8	0,00
Kegg	Hypo	Huntington's disease	8	0,00
Kegg	Hypo	Cardiac muscle contraction	5	0,00
Kegg	Hypo	Non-alcoholic fatty liver disease (NAFLD)	6	0,00
Kegg	Hypo	Metabolic pathways	17	0,01
Kegg	Hyper	Pancreatic secretion	4	0,02
Kegg	Hyper	Ribosome	5	0,03
Kegg	Hyper	Rap1 signaling pathway	5	0,03
Kegg	Hyper	Ras signaling pathway	5	0,03
Kegg	Hyper	Pancreatic cancer	3	0,08
Kegg	Hyper	Arachidonic acid metabolism	3	0,09
Kegg	Hyper	Colorectal cancer	3	0,09